5h. Electric and Magnetic Fields in the Earth's Environment

M. SUGIURA AND J. P. HEPPNER

NASA-Goddard Space Flight Center

EARTH'S MAIN MAGNETIC FIELD

5h-1. Sources of the Magnetic Field at the Earth's Surface. The largest contribution to the magnetic field observed on the surface of the earth comes from its main field. The *main field* is considered to be produced in the earth's fluid core where the magnetic field and the convective motion of thermal origin are coupled to constitute a self-maintaining dynamo. The main field (Secs. 5h-4 and 5h-5) at the earth's surface is distorted to varying degrees by the earth's crustal anomalies (Sec. 5h-7) and by the magnetic fields from sources external to the solid earth. The latter include those from ionospheric currents (Secs. 5h-8 to 5h-10), effects of plasmas in the magnetosphere (Secs. 5h-11 and 5h-21), and the distortion of the magnetospheric magnetic field by the solar wind (Secs. 5h-12 and 5h-20).

5h-2. Units Conventionally Used in Geomagnetism [1]. Except in dealing with magnetic material, the magnetic permeability is unity in cgs units, and thus the distinction between magnetic induction **B** and magnetic field intensity **H** can be dispensed with without confusion. Hence, although the cgs unit for **H** is *oersted*, the unit for **B**, namely *gauss* (Γ), is conventionally used for both **B** and **H**. For weak magnetic fields and for describing time variations of the field, the unit *gamma* (γ) is used, where $1\ \gamma = 10^{-5}$ Γ. Declination and inclination are expressed in angular measure, normally in degrees and minutes.

5h-3. Component Nomenclature [1,2]. The magnetic field vector is described by three orthogonal components, by the magnitude and two angles specifying the direction, or by a mixture of these. The standard nomenclature in geomagnetism is as follows:

- X, Y, and Z — three components measured positively northward, eastward, and vertically downward, respectively
- B (or F) — the magnitude of the field vector, (also called total force or intensity) $F = (X^2 + Y^2 + Z^2)^{\frac{1}{2}}$
- H — the magnitude of the horizontal intensity, $H = (X^2 + Y^2)^{\frac{1}{2}}$
- D — declination: the angular deviation of the horizontal projection of the field vector from geographic north, taken positive when eastward, $D = \tan^{-1}(Y/X)$
- I — inclination, or dip angle: the inclination of the field vector from the horizontal plane, taken positive when downward, $I = \tan^{-1}(Z/H)$

5h-4. Dipole Description of the Main Field [1–3]. The main field is described, to a first approximation, by the field of a magnetic dipole placed at the earth's center (i.e., a *centered dipole*) with the following equations and parameters [4]:

$$H = H_0 \left(\frac{a}{r}\right)^3 \sin\Theta$$

$$Z = 2H_0 \left(\frac{a}{r}\right)^3 \cos\Theta$$

$$M = H_0 a^3$$

where M = 8.0052 × 10^{25} gauss cm^3, the dipole moment
H_0 = 0.30953 gauss, the field intensity at the magnetic equator ($I = 0°$, $\Theta = 90°$) for $r = a$
a = 6371.2 km, the reference radius for a spherical earth
r = radial distance, km, from the earth's center
Θ = geomagnetic colatitude, from the geomagnetic coordinate system, below

Geomagnetic coordinates (Θ and Λ, respectively, for geomagnetic colatitude and east longitude) are given in terms of geographic coordinates (θ and λ, respectively, for geographic colatitude and east longitude) by

$$\cos\Theta = \cos\theta\cos\theta_0 + \sin\theta\sin\theta_0\cos(\lambda - \lambda_0)$$
$$\sin\Lambda = \sin\theta\sin(\lambda - \lambda_0)/\sin\Theta$$

where [4] θ_0 = 11.44°, the geographic colatitude of the north *geomagnetic pole* (also called the north *dipole pole*);
λ_0 = 290.24°, the geographic east longitude of the north geomagnetic pole

The errors in describing the magnetic field at the earth's surface by means of the above centered dipole are as great as 10 percent in some regions. For a somewhat more accurate dipole description some use has been made of an *eccentric dipole* [5] representation in which a dipole is located at a position displaced from the earth's center. This is equivalent to adding the potential terms for g_2^1, h_2^1, g_2^2, and h_2^2 from the spherical harmonic description (Sec. 5h-5) to the potential term $H_0\cos\theta$ for the centered dipole. As indicated by the $(a/r)^{n+1}$ dependence of the potential in the spherical harmonic description (Sec. 5h-5), the errors in describing the main field by means of a dipole decrease rapidly with increasing distance r from the earth.

The study of phenomena related to the interaction between the geomagnetic field and the solar wind (Secs. 5h-10 to 5h-12), including many of the indirect effects of this interaction, is often facilitated by use of the parameter geomagnetic local time in place of either local mean or standard time. This is a consequence of the magnetic field being symmetrical, to a first approximation, about the magnetic axis rather than the geographic axis. *Geomagnetic Local Time* [1,2] is defined analogous to the conventional local time system by replacing the geographic axis with the geomagnetic axis and defining *geomagnetic noon* for a location P as being the time when the subsolar point lies on the geomagnetic meridian of P. Geomagnetic Local Time for any location P is thus given in angular measure by $180° + \Lambda_P - \Lambda_S$, where Λ_P and Λ_S are the geomagnetic longitudes of the location P and the subsolar point, respectively.

An additional coordinate parameter which has been effective in organizing the data on geomagnetic phenomena related to particle motions in space is the *invariant latitude*, $\Psi = \cos^{-1} 1/L^{\frac{1}{2}}$. Here, L is the shell parameter defined in Sec. 5h-22 that gives the distance in the geomagnetic equatorial plane (in units of earth radii R_e) to a field line having its intercept at the earth's surface at the invariant latitude Ψ. Although L, and thus Ψ, is usually computed from a spherical harmonic field description (Sec. 5h-5), it is noted here because invariant latitude is frequently used in place of the dipole geomagnetic latitude.

5h-5. Spherical Harmonic Description of the Main Field [1,2,5]. The main field can be described, outside its source region, by a scalar magnetic potential V satisfying Laplace's equation $\nabla^2 V = 0$. $\mathbf{B} = -\nabla V$ then defines the vector magnetic field. Expressed in a spherical harmonic series,

$$V = a\sum_{n=1}^{\infty}\left(\frac{a}{r}\right)^{n+1}\sum_{m=0}^{n} P_n^m(\cos\theta)\,(g_n^m\cos m\lambda + h_n^m\sin m\lambda)$$

where θ = geographic colatitude (see Sec. 5h-4 for other coordinate symbols).
$P_n^m(\cos\theta)$ = associated Legendre function of degree n and order m. The normalization introduced by Schmidt is most frequently used.
g_n^m, h_n^m = constants called the *Gauss coefficients*.
The vector components of the magnetic field (Sec. 5h-3) are given by

$$X = \frac{1}{r}\frac{\partial V}{\partial \theta}$$

$$Y = -\frac{1}{r \sin\theta}\frac{\partial V}{\partial \lambda}$$

$$Z = \frac{\partial V}{\partial r}$$

X and Z above are applicable to a spherical earth; for accurate evaluations of X and Z on the surface of the actual earth, its oblateness should be taken into account.

TABLE 5h-1. GAUSS COEFFICIENTS FOR THE INTERNATIONAL GEOMAGNETIC REFERENCE FIELD [4] FOR EPOCH 1965.0*
(Units: gammas)

n	m	g_n^m	h_n^m	n	m	g_n^m	h_n^m
1	0	−30,339	0	6	2	4	106
1	1	−2,123	5,758	6	3	−229	68
2	0	−1,654	0	6	4	3	−32
2	1	2,994	−2,006	6	5	−4	−10
2	2	1,567	130	6	6	−112	−13
3	0	1,297	0	7	0	71	0
3	1	−2,036	−403	7	1	−54	−57
3	2	1,289	242	7	2	0	−27
3	3	843	−176	7	3	12	−8
4	0	958	0	7	4	−25	9
4	1	805	149	7	5	−9	23
4	2	492	−280	7	6	13	−19
4	3	−392	8	7	7	−2	−17
4	4	256	−265	8	0	10	0
5	0	−223	0	8	1	9	3
5	1	357	16	8	2	−3	−13
5	2	246	125	8	3	−12	5
5	3	−26	−123	8	4	−4	−17
5	4	−161	−107	8	5	7	4
5	5	−51	77	8	6	−5	22
6	0	47	0	8	7	12	−3
6	1	60	−14	8	8	6	−16

* Courtesy of J. C. Cain and S. J. Cain.

Table 5*h*-1 gives the Gauss coefficients for the International Geomagnetic Reference Field [4] for epoch 1965.0. Table 5h-2 gives a second set of coefficients determined directly from measurements by the *OGO*-2 and *OGO*-4 satellites [6] taken between October, 1965, and December, 1967, but referenced through use of secular change terms (Sec. 5h-6) to the same date, $t = 0$ at time 1965.0. Comparison of different sets of coefficients gives an indication of the accuracy of spherical harmonic descriptions of the main field. The relatively uniform latitude and longitude distribution of data from the polar orbiting *OGO* satellites selected for magnetically quiet periods ($K_p = 0$, Sec. 5h-13) provides a data set suitable for examining differ-

TABLE 5h-2. GAUSS COEFFICIENTS BASED ON THE *OGO*-2 AND 4 SATELLITE DATA [6] AND REFERENCED TO EPOCH 1965.0*
(Units: gammas)

n	m	g_n^m	h_n^m	n	m	g_n^m	h_n^m
1	0	−30,338	0	8	3	−11	5
1	1	−2,114	5,768	8	4	−2	−18
2	0	−1,661	0	8	5	5	6
2	1	2,994	−2,013	8	6	−6	20
2	2	1,597	103	8	7	12	−3
3	0	1,298	0	8	8	10	−22
3	1	−2,041	−403	9	0	10	0
3	2	1,295	237	9	1	8	−22
3	3	856	−169	9	2	2	15
4	0	956	0	9	3	−12	4
4	1	807	153	9	4	14	−2
4	2	480	−269	9	5	0	−3
4	3	−387	16	9	6	0	10
4	4	200	−274	9	7	2	13
5	0	−221	0	9	8	4	1
5	1	360	17	9	9	0	4
5	2	250	128	10	0	−3	0
5	3	−33	−127	10	1	−2	2
5	4	−152	−100	10	2	2	1
5	5	−61	99	10	3	−5	2
6	0	46	0	10	4	−2	6
6	1	60	−11	10	5	7	−4
6	2	8	104	10	6	6	1
6	3	−229	70	10	7	0	−2
6	4	−3	−31	10	8	0	4
6	5	4	−12	10	9	2	3
6	6	−100	0	10	10	0	−10
7	0	71	0	11	0	2	0
7	1	−53	−62	11	1	−1	1
7	2	3	−27	11	2	−2	3
7	3	14	−6	11	3	4	−1
7	4	−31	7	11	4	−1	−3
7	5	−3	19	11	5	1	0
7	6	12	−24	11	6	−1	−1
7	7	3	−26	11	7	1	−2
8	0	10	0	11	8	2	−1
8	1	5	9	11	9	−1	−4
8	2	−4	−13	11	10	4	−1
				11	11	3	3

* Courtesy of J. C. Cain and S. J. Cain.

ences between calculated and measured values—particularly because the data, at altitudes >400 km, is not significantly affected by the crustal anomalies described in Sec. 5h-7. Using the *OGO* set of coefficients, the root-mean-square values of the residuals in scalar B for the difference (measured minus computed) for *OGO*-2 and *OGO*-4 data are 7 and 9 γ, respectively. The corresponding rms residuals, using the coefficients adopted for the International Geophysical Reference Field, are 39 and 57 γ, respectively.

Figure 5h-1 illustrates the form of the main magnetic field at the earth's surface in terms of the total scalar intensity B. The lack of dipole symmetry and the possible ambiguity of using the term magnetic pole without further definition are evident features. The preferred terminology is to use the term *dip pole* when referring to the

location where $I = 0°$ and the term *geomagnetic pole*, or *dipole pole* (Sec. 5h-4), when referring to the surface intercepts of the axis of the centered dipole determined from the coefficients g_1^0, g_1^1 and h_1^1. It is further evident that pole positions do not correspond to locations of maximum field intensity.

5h-6. Secular Variations of the Main Field [1,2,7–9]. The main magnetic field as observed at the earth's surface varies noticeably on a time scale of several or more years. These changes are called the *secular variations*. The secular variations can be represented by maps with contours of equal rate of change for various quantities.

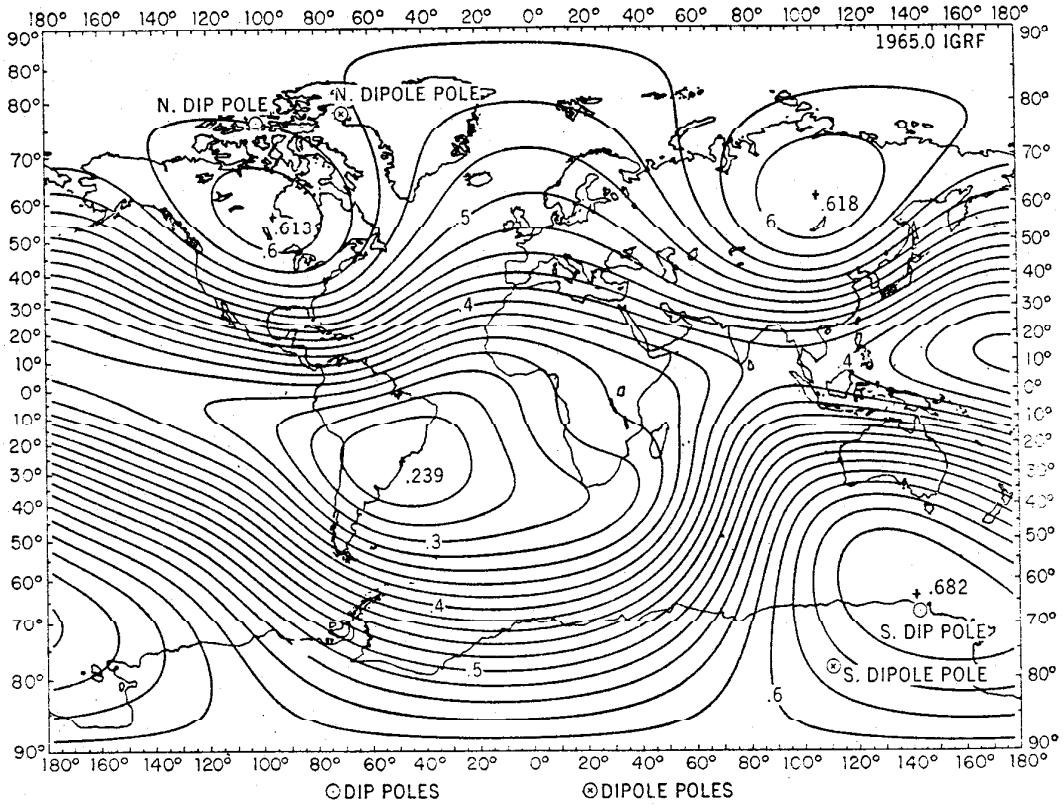

FIG. 5h-1. The earth's main magnetic field (Sec. 5h-5): the distribution of the magnitude B on the earth's surface as calculated from the 1965.0 International Geomagnetic Reference Field (Table 5h-1); B measured in gauss. (*Courtesy of S. J. Cain.*)

Such contours for the total force B are referred to as *isopors;* an example of an isopor chart for the epoch of 1965 is shown in Fig. 5h-2.

The secular variation is also expressed by regarding the Gauss coefficients (Sec. 5h-5) as being time-dependent [10]. The coefficients g_n^m and h_n^m are then replaced, respectively, by $g_n + \dot{g}_n^m t$ and $h_n^m + \dot{h}_n^m t$, where t is time measured in years from a specific epoch date. The coefficients $\dot{g}_n^m$ and $\dot{h}_n^m$ are given in Table 5h-3 for epoch 1965.0 for the International Geomagnetic Reference Field.

The nondipole part of the main field as expressed by the spherical harmonics for different epochs appears to indicate the presence of two types of gross features: (1) regions over which the pattern of deviations from a dipole field has remained relatively constant through the history of accurate measurements, and (2) regions over which the pattern of deviations appears to be drifting westward at rates of 0.2 to 0.3 deg/year. The analyses also suggest a poleward shifting of the dipole field as indicated by a change

of 24 γ/year in the term dg_2^0/dt (Table 5h-3) of the harmonic analysis which is the largest change observed in any single coefficient. There are also indications that the dipole moment (Sec. 5h-4) has decreased at a relatively uniform rate from about 8.55×10^{25} gauss cm^3 in 1835 [5] to 8.005×10^{25} in 1965.

5h-7. Crustal Anomalies [8,11,12]. The main magnetic field is locally distorted at the earth's surface by differences in the degree of magnetization of various rock formations. This magnetization is primarily dependent on the magnetite, Fe_3O_4, content and exists to the depth at which the Curie temperature (575°C for magnetite) is reached. Over many regions of the earth this depth is estimated to be about 20 km,

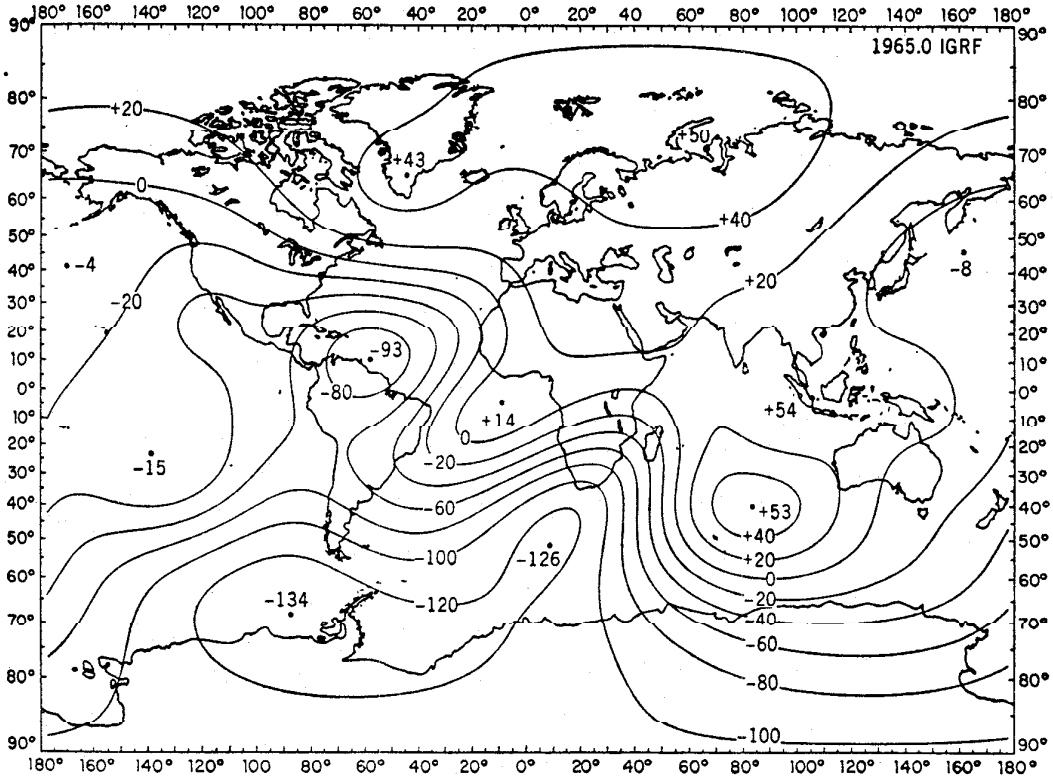

FIG. 5h-2. The secular variations (Sec. 5h-6) in the magnitude B of the main magnetic field: calculated from the secular variation terms in the 1965.0 International Geomagnetic Reference Field (Table 5h-3); units are gammas. (*Courtesy of S. J. Cain.*)

but variations in estimates range from 10 to 30 km. The magnetization is of two types: induced (proportional to the rock susceptibility and the main field **B**), and permanent (the remnant magnetization from a geologically earlier state of magnetization). Extensive mapping of magnetic anomalies has been carried out over many regions of the earth's surface to aid in inferring the subsurface geology. The distribution, intensity, and number of anomalies as a function of their dimensions are highly variable for different regions. However, considering dimensions >1 km, statistics indicate: (1) that the number of anomalies sharply decreases between anomaly dimensions of 25 and 50 km, (2) that between anomaly dimensions of 50 and 300 km the number of anomalies gradually decreases with increasing dimensions, and (3) that the comparatively small number of anomalies that have a maximum dimension >300 km usually appear in a lineation pattern that marks a major geologic boundary resulting from large-scale tectonic activity. On a similar scale (resolution about 1 km), anomaly intensities are statistically indicated by noting that contour

TABLE 5h-3. SECULAR VARIATION TERMS FOR EPOCH 1965.0 IN THE SPHERICAL HARMONIC EXPRESSION: BASED ON THE INTERNATIONAL GEOMAGNETIC REFERENCE FIELD [4]*
(Units: gammas/year)

n	m	$\dot{g}_n^m$	$\dot{h}_n^m$	n	m	$\dot{g}_n^m$	$\dot{h}_n^m$
1	0	15.3	0.0	6	2	1.1	−0.4
1	1	8.7	−2.3	6	3	1.9	2.0
2	0	−24.4	0.0	6	4	−0.4	−1.1
2	1	0.3	−11.8	6	5	−0.4	0.1
2	2	−1.6	−16.7	6	6	−0.2	0.9
3	0	0.2	0.0	7	0	−0.5	0.0
3	1	−10.8	4.2	7	1	−0.3	−1.1
3	2	0.7	0.7	7	2	−0.7	0.3
3	3	−3.8	−7.7	7	3	−0.5	0.4
4	0	−0.7	0.0	7	4	0.3	0.2
4	1	0.2	−0.1	7	5	−0.0	0.4
4	2	3.0	1.6	7	6	−0.2	0.2
4	3	−0.1	2.9	7	7	−0.6	0.3
4	4	−2.1	−4.2	8	0	0.1	0.0
5	0	1.9	0.0	8	1	0.4	0.1
5	1	1.1	2.3	8	2	0.6	−0.2
5	2	2.9	1.7	8	3	0.0	−0.3
5	3	0.6	−2.4	8	4	−0.0	−0.2
5	4	0.0	0.8	8	5	−0.1	−0.3
5	5	1.3	−0.3	8	6	0.3	−0.4
6	0	−0.1	0.0	8	7	−0.3	−0.3
6	1	−0.3	−0.9	8	8	−0.5	−0.3

* Courtesy of J. C. Cain and S. J. Cain.

maps are often prepared in units of 100 γ. Anomalies involving changes of several thousand gammas over horizontal distances of several tens of kilometers are considered to be strong anomalies.

SURFACE GEOMAGNETIC VARIATIONS OF SPACE ORIGIN

5h-8. Solar Daily Variation on Quiet Days [1–3]. The regular magnetic variation observed on an average magnetically quiet day is called the *Sq variation*. The source of *Sq* is a system of electric currents in the *E* region of the ionosphere (Sec. 5h-15). Systematic winds produced mainly by the solar heating of the atmosphere generate the current through a dynamo action which is effective between roughly 95 and 130 km where the electric conductivity is high. The relevant conductivity elements are given in Sec. 5h-18.

Examples of magnetograms on a typical quiet day are shown in Fig. 5h-3 for observatories at low and middle latitudes and near the dip equator. An illustrative picture of the *Sq* current system is shown in Fig. 5h-4. Within about 200 km of the dip equator, $I = 0°$ (Sec. 5h-3), the *Sq* range in *H* is very large, as indicated by the Huancayo, Peru, magnetogram in Fig. 5h-3. The concentrated ionospheric current along the dip equator on the day side of the earth which produces this large change in *H* is referred to as the *equatorial electrojet*. It results from an enhanced effective conductivity (Cowling conductivity, Sec. 5h-18) in the east-west direction in a narrow belt at the dip equator. Typical ranges in the magnitude of *Sq* at the earth's surface are roughly 50 to 250 γ at the dip equator and 30 to 60 γ at magnetic latitudes 10 to 60°. Both the form and magnitude of *Sq* can vary considerably from one day to the next and also with season and solar activity.

5h-9. Lunar Geomagnetic Variation [1,2]. The tidal oscillation of the atmosphere due to the gravitational force of the moon generates an electric current in the ionosphere which gives rise to the *lunar geomagnetic variation*, conventionally denoted by L. Amplitudes of L are about one-tenth of those of Sq, and are not generally recognizable in the magnetograms by the eye. An exception to this is L near the dip equator, where its amplitude is enhanced over the corresponding amplitudes at higher latitudes by a rate greater than that for the similar enhancement in Sq (Sec. 5h-8). The current system for L varies greatly with lunar phase and season. (*Note.* The use of L for lunar variations is not related to the L shell parameter described in Sec. 5h-22.)

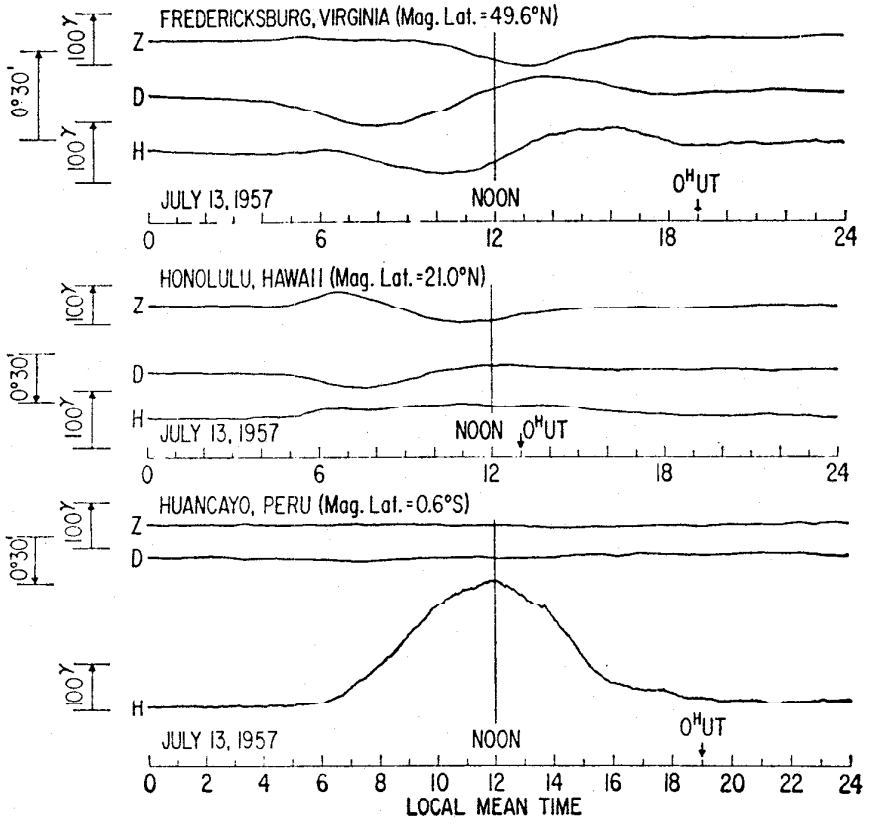

FIG. 5h-3. Typical magnetograms on a quiet day, showing the solar daily variation Sq (Sec. 5h-8). H is the horizontal component, D the declination, and Z the vertical component. The H trace for Huancayo shows the effect of the equatorial electrojet.

5h-10. High-latitude Magnetic Disturbances [2,3,13,14]. At high latitudes the magnetic field is disturbed more frequently and more severely than at middle and low latitudes. Disturbances are statistically greatest along oval-shaped belts encircling the dipole poles in each hemisphere roughly at Θ (or $90° - \Psi$) = 15 to 20° near noon, 17 to 23° near the twilight meridians, and 19 to 26° near midnight [15–17]. (*Note.* Θ is used in this section as geomagnetic colatitude for each hemisphere.) As the ionospheric electric currents causing the magnetic disturbances in these belts are associated with the occurrence of aurora, they are usually referred to as the *auroral belts* or *auroral ovals* [18]. Within these belts maximum disturbance intensities are most commonly encountered at Θ = 20 to 25° in the nighttime geomagnetic local time range (Sec. 5h-4) 20^h to 04^h. The frequency of occurrence of aurora is also a maximum in these nighttime strips, and this statistic has led to the designation

of the strips centered near $\Theta = 23°$ as the *auroral zones*. The colatitudes Θ indicated above decrease by several degrees during times of weak activity and increase during times of intense activity and magnetic storms. During intense storms values of Θ as great as 35° are not uncommon in the midnight sector.

Figure 5h-5 is an idealized representation of the distribution of ionospheric electric currents for a disturbance of moderate intensity (*Note.* Because current may also flow along magnetic field lines to magnetospheric regions, currents are not drawn as being continuous within the ionosphere.) Several major features to note are: (1) The most intense current flows westward in the auroral belt toward the 22^h to 23^h region from the morning sector. This concentration of current is often called the

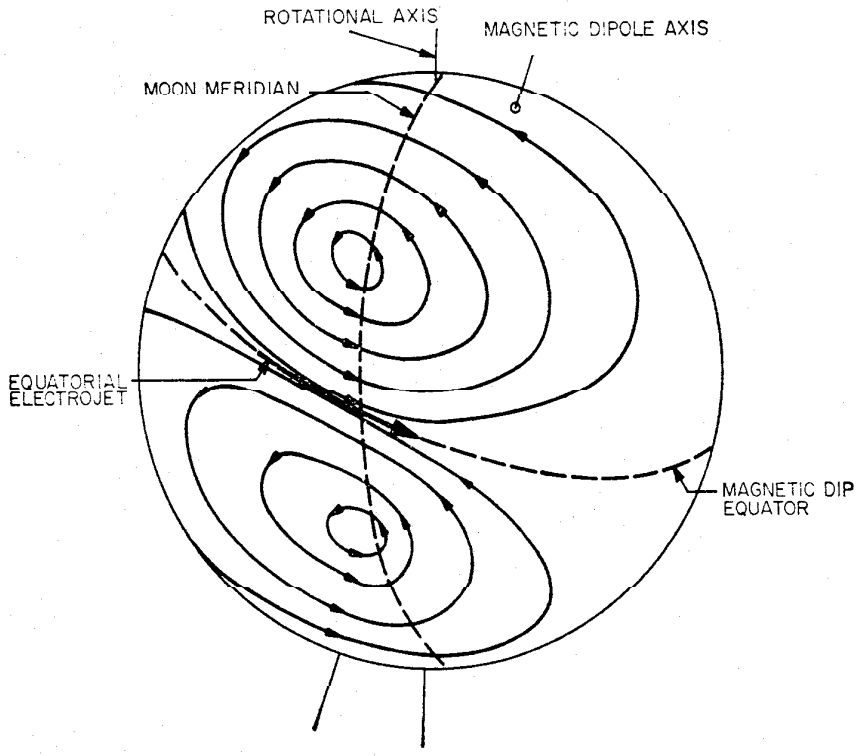

FIG. 5h-4. Illustration of the ionospheric current system for the solar daily variation S_q (Sec. 5h-8); the stronger current vortex represents the average condition in northern summer.

auroral electrojet. (2) A weaker auroral electrojet current flows eastward toward the 22^h to 23^h region from the evening sector. (3) A comparatively uniform current flows across the *polar cap* (the region poleward from minimum Θ for the auroral belt) from the late evening sector to the late morning sector. (4) Much weaker currents spread outward to the middle-latitude regions. Although shown only for one hemisphere, the same distribution occurs simultaneously in the other hemisphere, indicating that the magnetic field lines connecting the two auroral belts are also lines of electrical equipotentials in the electric field system (Sec. 5h-28) driving the electrojet currents. Sounding rocket measurements have shown that the auroral electrojets are primarily Hall currents (Sec. 5h-18) driven by horizontal electric fields (Sec. 5h-28) in the region of the ionosphere where energetic electrons precipitate from the magnetosphere and increase the ionization and hence the conductivity.

Enhancements of these disturbances typically last one to several hours and are often repeated at intervals of several hours. Disturbances of this type are sometimes

referred to as *magnetic bays* (a term originating from the resemblance of the H trace on magnetograms during such events to the coastline of a bay on a map). Directly beneath the auroral electrojets, variations are largest in the H component and usually lie within the range 100 to 1,000 γ, but may on occasions reach values greater than 2,000 γ. Large bay disturbances often occur during magnetic storms (Sec. 5h-11). The magnetic activity indices K_p and AE (Sec. 5h-13) are essentially measures of the severity of magnetic disturbances in the auroral belt.

5h-11. Magnetic Storms [1,2,19]. Worldwide magnetic disturbances lasting one to several days are called *magnetic storms*. Magnetic storms often, but not always, begin with a sudden, worldwide increase in the magnetic field. This sudden field increase, called a *sudden commencement* and denoted by *SC*, is due to a compression of

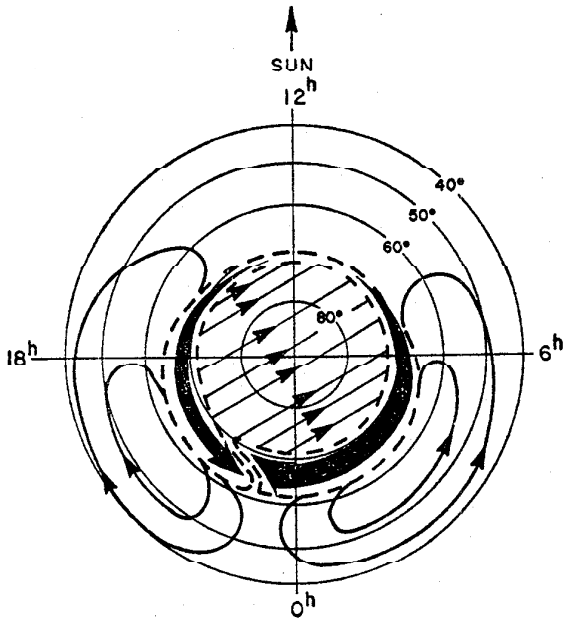

FIG. 5h-5. Illustration of ionospheric currents for a high-latitude disturbance. Concentric circles represent geomagnetic latitude ($90° - \theta$) circles.

the magnetosphere by a sudden increase in the pressure on the magnetosphere boundary exerted by the solar wind; magnetic variations of this type are discussed in Sec. 5h-12. Examples of magnetograms taken during a magnetic storm are shown in Fig. 5h-6.

Typically, one-half to a few hours after an *SC* the magnetic field begins to decrease all over the globe, and after reaching a minimum in several hours recovers slowly toward the prestorm level. The field decrease, often called a *Dst* decrease (Sec. 5h-13) is due to a creation of a plasma belt at a distance of 2.5 to 6 earth radii [20]. The plasma belt exerts magnetic stress such that the magnetic field in the magnetosphere is inflated, resulting in a field decrease inside the plasma belt and an increase outside it [21]. In the developing phase of a magnetic storm the plasma belt grows most rapidly in the late afternoon sector of the magnetosphere, and consequently the field decrease observed on the earth is also larger in this sector than in other sectors. The magnetic stress of the plasma belt mainly comes from its protons in the energy range 10 to 100 kev.

During magnetic storms high-latitude disturbances of the type discussed in Sec. 5h-10 occur in greater intensity than under normal conditions (e.g., see College, Alaska, in Fig. 5h-6). Field variations produced by an auroral electrojet may reach 3,000

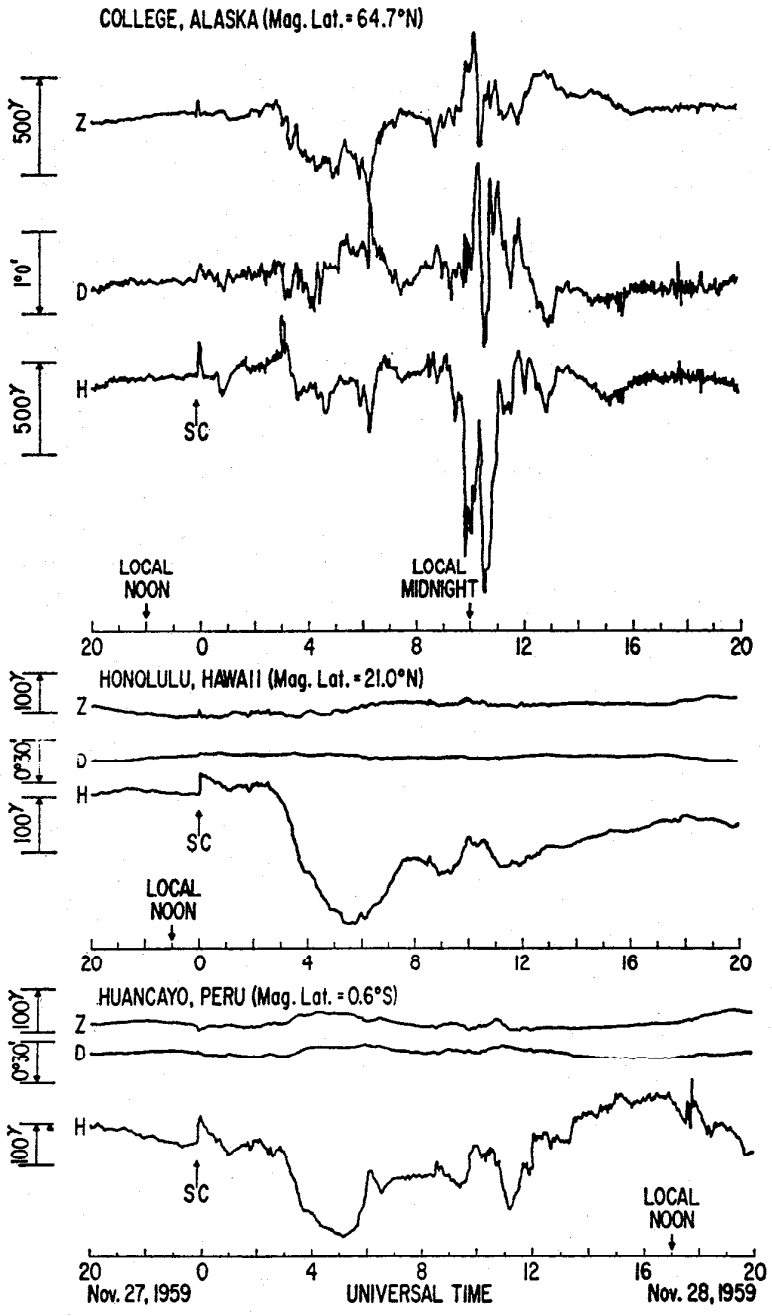

FIG. 5h-6. Magnetograms taken during a magnetic storm (Sec. 5h-11): examples from high-latitude (top) and low-latitude (middle and bottom) stations.

γ during an exceptionally large storm. In such a storm the *Dst* decrease may exceed 400 γ.

The frequency of occurrence and the average intensity of magnetic storms are statistically correlated with solar activity. However, individual magnetic storms can by no means be traced to active regions on the sun, and conversely solar flares do not always produce magnetic storms on the earth. During the International Geophysical Year, July, 1957, to December, 1958, representing a period of maximum solar activity, magnetic storms with *Dst* decreases exceeding 40 γ occurred at a rate of 55 storms per year, and the average *Dst* decrease was 110 γ, with a maximum of

434 γ observed on September 13, 1957, which was still the largest (as of November 1, 1968) since 1957. In 1964 a year of solar activity minimum, there were only 15 magnetic storms (as defined above), and the average *Dst* decrease of these storms was 61 γ, with a maximum of 109 γ [22,23].

5h-12. Magnetic Variations Caused by Compressions and Expansions of the Magnetosphere. Compression or expansion of the magnetosphere responding to an increase or decrease of the solar wind pressure on its boundary surface produces a class of magnetic variations of considerable interest, in spite of their generally small magnitudes. Sudden commencements (*SC*) of magnetic storms (Sec. 5h-11) and *sudden impulses* belong to this class. A sudden impulse, often denoted by *SI*, is a sudden increase or decrease in the magnetic field observed simultaneously over the world [2].

The theoretical magnetic field change ΔB at the ground is related to changes in the proton density n and the velocity v of the solar wind approximately by the formula [24]

$$\Delta B = 0.03\Delta(n^{\frac{1}{2}}v)$$

where ΔB is in γ, n in protons/cm^3, and v in km/sec. For sudden commencements ΔB ranges from several to 100 γ, whereas ΔB for sudden impulses is normally less than 20 γ. The effect of an abrupt compression of the magnetosphere boundary is transmitted inward hydromagnetically [25]. Presence of continuous time variations in *Dst* (Sec. 5h-13) with appreciable amplitudes suggests that occurrences of more gradual, as compared with sudden, compression or expansion of the magnetosphere are not infrequent, but their significance has not as yet been explored.

5h-13. Magnetic Indices [1,26,27]. *Planetary 3-hourly Index Kp.* The *Kp* index expresses the intensity of geomagnetic activity mainly at high latitudes (Sec. 5h-10) for each 3-hr interval of the Greenwich day, in a scale of thirds in the order:

$$0o \quad 0+ \quad 1- \quad 1o \quad 1+ \quad 2- \quad 2o \quad 2+ \cdots 8- \quad 8o \quad 8+ \quad 9- \quad 9o$$

which may be condensed to a scale of integers from 0 to 9. *Kp* is based on magnetic records from 12 selected observatories lying between 47.7 and 62.5° dipole latitude with the average of 56°. The *Kp* index is published regularly by the International Association of Geomagnetism and Aeronomy in the No. 12 series of its Bulletin. Indices *ap*, *Ap*, *Ci*, *Cp*, etc., are also found in the same publication.

Three-hourly Equivalent Planetary Amplitudes, ap. The conversion from *Kp* to *ap* is made according to the following table:

Kp =	0o	0+	1−	1o	1+	2−	2o	2+	3−	3o	3+	4−	4o	4+
ap =	0	2	3	4	5	6	7	9	12	15	18	22	27	32
Kp =	5−	5o	5+	6−	6o	6+	7−	7o	7+	8−	8o	8+	9−	9o
ap =	39	48	56	67	80	94	111	132	154	179	207	236	300	400

At a standard station the average range of the most disturbed of the three magnetic components is 2 *ap* (γ); for instance, if $Kp = 6+$, the range is 188 γ. The scale for *ap* is linear, while that for *Kp* is quasi-logarithmic.

Daily Equivalent Planetary Amplitude, Ap. The average of the eight values of *ap* for each day is the daily equivalent planetary amplitude *Ap*. Hence *Ap* is also expressed in units of 2 γ for a standard station.

Daily International Character Figure Ci, and Daily Planetary Character Figure Cp. The daily international character figure *Ci* is the average of the daily character figure *C* for all collaborating observatories; *Ci* varies from 0.0 to 2.0. *Ci* is available for every day since 1884.

A more recently introduced substitute index Cp is derived from the daily sum of ap according to the following scheme.

ap sum up to:

	22	34	44	55	66	78	90	104	120	139	164	190	228
Cp =	0.0	0.1	0.2	0.3	0.4	0.5	0.6	0.7	0.8	0.9	1.0	1.1	1.2

ap sum up to:

	273	320	379	453	561	729	1119	1399	1699	1999	2399	3199	3200
Cp =	1.3	1.4	1.5	1.6	1.7	1.8	1.9	2.0	2.1	2.2	2.3	2.4	2.5

Though values of Ci and Cp are found to be nearly the same, Cp is more reliable and should be used in preference to Ci.

Auroral Electrojet Index AE [28]. The AE index is designed to be a measure of global auroral electrojet activity with higher time resolution than Kp. The index is normally given at 2.5-min intervals, but hourly averages are also used. AE represents the instantaneous range of disturbance of the horizontal component H from a set of observatories that are relatively uniformly distributed in longitude between magnetic colatitudes Θ of 30 and 19°. $AE = \Delta H$ (maximum) + $|\Delta H$ (minimum)|, where ΔH (maximum) is taken from the observatory showing the maximum positive deviation of H, and $|\Delta H$ (minimum)| is taken from the observatory showing the largest negative value in H.

Dst Index [22]. The component of disturbance magnetic field that is axially symmetric with respect to the geomagnetic dipole axis is called *Dst*. The *Dst* index, computed at hourly or 2.5-min intervals, is useful for studies of magnetic storm phenomena (Sec. 5h-11). $Dst = 1/n\ (\Delta H_1 + \Delta H_2 + \cdots + \Delta H_n)$ represents the average deviation of the horizontal component from quiet-day values for a set of n observatories that are relatively uniformly distributed in longitude and located at low ($<35°$) magnetic latitudes.

5h-14. Induced Currents in the Earth [1,29–31]. Since the solid earth is a good conductor, currents are induced within the earth by any time-varying magnetic field changes imposed on it; and these induced currents in turn modify the field changes observed on and above the earth. For magnetic fields applied from sources external to the earth, the longer the periods of the changes, the greater the depth of the penetration of the fields. This property is used to estimate the conductivity distribution within the earth; a method frequently used is to assume a model with a set of parameters which are to be determined so as to fit the observed variations on the earth. In the case of slow variations such as Sq, approximately two-thirds of the variation observed on the earth is directly from the currents in the ionosphere, and one-third from the currents induced in the earth. A simple conductivity model often used assumes a uniform, conducting sphere surrounded by a less conducting shell. Using Sq and disturbance fields of various periods, the conductivity in this sphere in such a model has been estimated to be of the order of 10^{-1} mho meter^{-1}; values of this magnitude may be considered as giving conductivities for the region roughly from 500 to 1,000 km depth. Estimates of conductivity in the lower mantle are based on studies of secular variations (Sec. 5h-6) or on direct calculations of conduction processes in rocks and minerals; though the reliability of these estimates is uncertain, values of the order of 10^2 mho meter^{-1} have been given. In the earth's molten core (below about 2,900 km depth) where the dynamo mechanism is thought to be operative maintaining the earth's field, conductivity estimates of the order of 10^5 to 10^6 mho meter^{-1} have been suggested. Upper mantle conductivity seems to have regional anomalies which can make various types of transient geomagnetic variations appear

quite different at stations close together. Near the surface of the earth the crustal conductivity can vary from one region to another by a large factor, since the conductivity depends on the type of rocks, mineral contents, temperature pressure, and water content. The most significant variables are the water content and its salinity. Such factors as regional variations in the thickness of the crust and the dependence of the conductivity on the frequency of incident electromagnetic waves further make a general statement on the crustal conductivity virtually impracticable. Effects of the electromagnetic induction in the oceans are not negligible in certain types of geomagnetic variations.

IONOSPHERE

5h-15. General [2,32–34]. The *ionosphere* extends from about 50 km above the ground to altitudes at which hydrogen ions become the main ion constituent. However, the definitions of the upper and lower boundaries of the ionosphere and its divisions into several regions, C, D, E, and F, are made for conventional, and not necessarily physically compelling, reasons.

The C region, extending to about 70 km height, is produced mainly by cosmic rays, and its peak electron density near 65 km height is of the order of 10^2 electrons cm^{-3}. Above the C region the ionization is due to the solar radiation with wavelengths from 1215.7 Å (for Lyman α of neutral hydrogen) to those of X rays. Altitudes from approximately 70 to 90 km are referred to as the D region, where the main ion constituents are NO^+ with O_2^+ and N_2^+ as secondary members. Hydrogen Lyman α is the main ionizing agency for NO^+. The peak electron density of the D region is of the order of 10^3 electrons cm^{-3} at 75 to 80 km height. Negative ions, particularly O_2^-, NO_2^-, and NO_3^-, are abundant in the nighttime D region. Their concentration decreases greatly in daytime as a consequence of photodetachment of the electrons in sunlight. The E region extends from about 90 to 140 km height. The ions there are mainly NO^+ and O_2^+, with N_2^+ ions as a secondary constituent. The steep increase in the electron density in the lower part of the E region is due to the ionization by X rays. Hydrogen Lyman β at 1025.6 Å and CIII at 976 Å are also important ionizing agencies. The maximum electron density in the E region is of the order of 10^5 electrons/cm^3 (see Sec. 5h-16 for electron density profiles). The F region, beginning from the top of the E region near 140 km height, has its peak electron density of the order of 10^6 electrons cm^{-3} between approximately 200 and 400 km height. The region above this F peak is often referred to as the *topside ionosphere.* The main ion constituent in the F region is O^+, mainly produced by EUV radiation in the wavelength range 300 to 800 Å. Although there is no agreed upper boundary for the F region, this may be taken to be the altitude beyond which hydrogen ions become the predominant ion constituent. This altitude depends upon the temperature, but is typically near 1,000 km; the region above this height is often called the *protonosphere.* In the transition from the region where O^+ ions are predominant to the region where H^+ ions take over, He^+ ions may become the predominant constituent.

The F region is sometimes divided into F_1 and F_2 layers because of the apparent ledge in the electron density profile, e.g., as seen in Fig. 5h-7. However, it is questionable if this separation is physically definable.

5h-16. Electron Density Profiles. The electron density profile in the ionosphere is variable to a great extent with latitude, local time, season, and solar activity. Several examples of these variations are shown in Fig. 5h-7. Variations in the ionospheric electron density involve considerable complexity; for instance, its diurnal variation is generally not symmetric with respect to local noon. The height distribution of the electron density in the F region is determined by a combination of photochemical equilibrium and diffusive equilibrium. The global distribution of the F-region electron

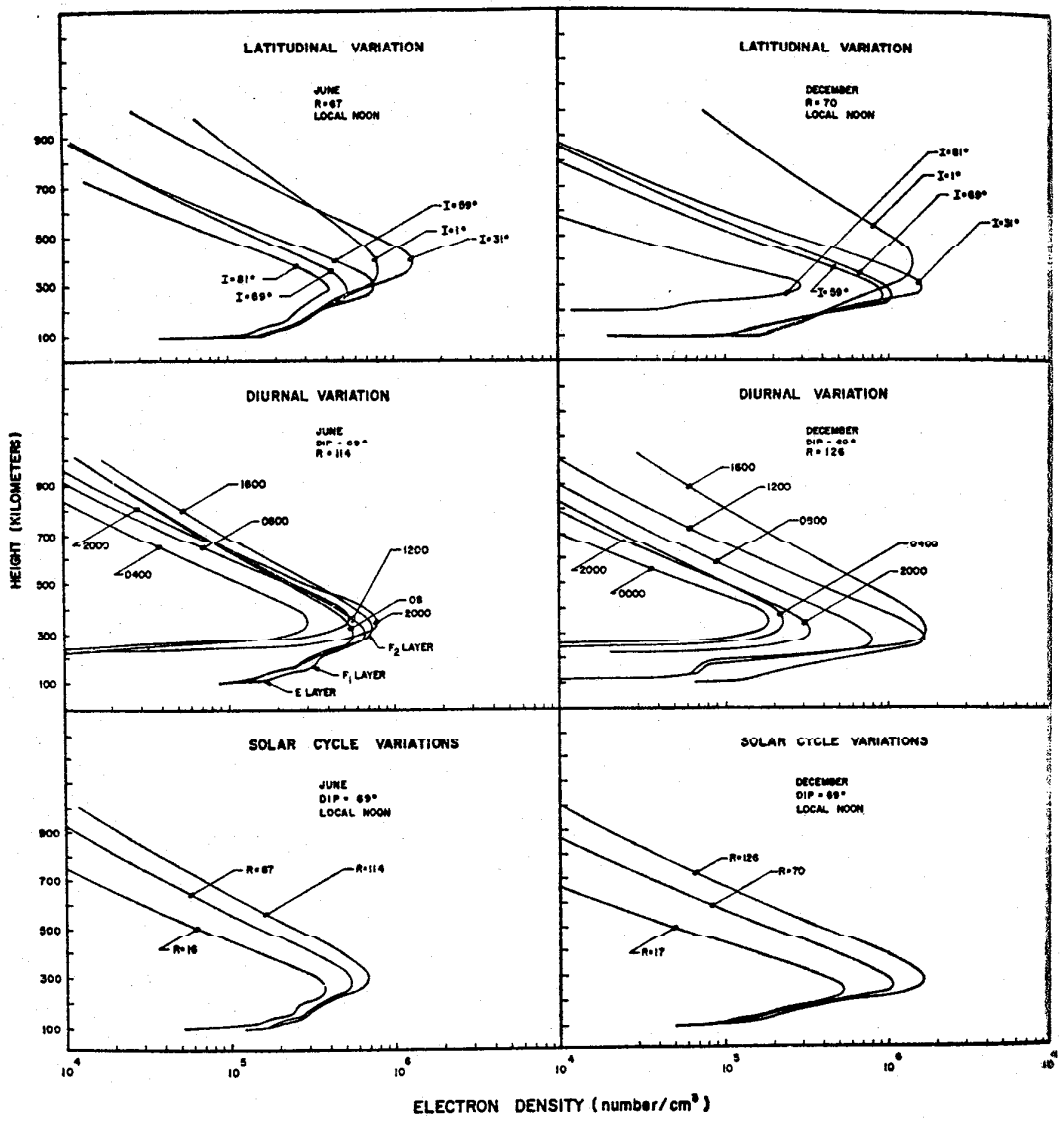

FIG. 5h-7. Monthly median electron density profiles (Sec. 5h-16): latitudinal, diurnal, and solar cycle variations. Below the peak of the F region the profiles were derived from ionograms, and above this altitude they were extrapolated exponentially. The stations used for the magnetic dip angles of 1, 31, 59, 69, and 81° are Huancayo, Bogota, Grand Bahama, Wallops Island, and Godhaven, respectively. (*Courtesy of T. E. VanZandt and A. R. Laird.*)

density is controlled to an appreciable degree by the geomagnetic field through its influence on the mass transport of ionization. An example of this nature is the "equatorial anomaly" exhibiting a minimum electron density over the magnetic equator and two maxima about 20° off, and on both sides of, the equator. Other outstanding anomalous characteristics of the F-region electron density include the high electron densities at middle latitudes near December in both hemispheres, i.e., the "December anomaly," and the larger electron densities in local winter than in summer, i.e., the "winter anomaly."

5h-17. Ionospheric Irregularities [35–37]. A variety of irregularities in the electron density distribution have been recognized as resulting from dynamical behavior involving ionospheric wind shears, particle precipitation from the magnetosphere, electrostatic wave instabilities, ionization by meteoritic impact, etc. Several of the most common types are noted below.

Thin horizontal layers of abnormally high electron density and sharp ledges in the electron density altitude profile are frequently found within the regular E region. These layers are called *sporadic E* [38,39] and denoted by E_S. The layers are often only several hundred meters to a few kilometers in thickness at temperate latitudes where they are thought to be produced primarily by wind shears. In auroral regions sporadic E occurs in many forms involving patches and magnetic field aligned irregularities of highly variable thickness. The combined effect of nonuniform particle precipitation from the magnetosphere and drift-wave instabilities in the ionosphere is largely responsible for the complexity of the auroral ionization which is called *auroral sporadic E*. In association with visible aurora the electron density is found to be roughly proportional to the square root of the optical brightness of the most prominent visible auroral emissions. Over the magnetic dip equator, embedded in the equatorial electrojet, sporadic-E ionization occurs in the form of magnetic field aligned irregularities of small dimensions (<1 meter to hundreds of meters) and small density contrast (approximately 1 percent). These *equatorial irregularities*, which are effective as low-frequency radar reflectors, are believed to be the result of a plasma instability which is closely related to the intensity of the equatorial electrojet current (Sec. 5h-8).

In, and above, the F region, *magnetic field aligned irregularities* are particularly prevalent over the polar caps and auroral belts. Although broken up into filamentary columns with cross-section dimensions of roughly 0.1 to 2 km, the individual filaments are probably >100 km in length. Density contrasts between adjacent filaments can involve changes by factors of 2, but contrasts of the order of 1 to 10 percent are much more common. When observed from the ground using radio sounding techniques, these irregularities give the normal F region the appearance of being spread upward. The term *spread F* has been commonly used to describe this appearance of the F region. Spread F is also observed frequently over the magnetic dip equator but appears to be more confined to F-region altitudes.

5h-18. Electric Conductivity in the Ionosphere [2,40,41]. Because of the low collision frequencies and of the presence of the strong magnetic field, the conductivity in the ionosphere above 70 km height is highly anisotropic for low-frequency electromagnetic waves and for d-c electric fields. Writing the current density $\mathbf{j}$ as

$$\mathbf{j} = \sigma_0 \mathbf{E}_\parallel + \sigma_1 \mathbf{E}_\perp + \sigma_2 (\hat{\mathbf{B}} \times \mathbf{E})$$

where $\mathbf{B}$ = magnetic induction
$\mathbf{E}$ = electric field intensity
$\hat{\mathbf{B}} = \mathbf{B}/|\mathbf{B}|$
$\mathbf{E}_\parallel = (\mathbf{E} \cdot \hat{\mathbf{B}})\hat{\mathbf{B}}$ = electric field intensity parallel to $\mathbf{B}$
$\mathbf{E}_\perp = \mathbf{E} - \mathbf{E}_\parallel$ = electric field intensity perpendicular to $\mathbf{B}$

The conductivity elements σ_0, σ_1, and σ_2 are called the *direct* (or *longitudinal*), *Pedersen*, and *Hall conductivities*, respectively. For electromagnetic waves of frequency ω, conductivities σ_0, σ_1, and σ_2 are respectively given, in mks units, by

$$\sigma_0 = ne^2\left[\frac{1}{m_e(\nu_e - i\omega)} + \frac{1}{m_i(\nu_i - i\omega)}\right]$$

$$\sigma_1 = ne^2\left\{\frac{\nu_e - i\omega}{m_e[(\nu_e - i\omega)^2 + \omega_e^2]} + \frac{\nu_i - i\omega}{m_i[(\nu_i - i\omega)^2 + \omega_i^2]}\right\}$$

$$\sigma_2 = ne^2\left\{\frac{\omega_e}{m_e[(\nu_e - i\omega)^2 + \omega_e^2]} - \frac{\omega_i}{m_i[(\nu_i - i\omega)^2 + \omega_i^2]}\right\}$$

where n = electron density in electron-ion pairs/m^3
e = electronic charge in coulombs
$m_{e,i}$ = electron, or ion, mass in kilograms
$\omega_{e,i} = eB/m_{e,i}$ = cyclotron (or gyro) frequency in radians/sec

The d-c conductivity is obtained by setting $\omega = 0$. In the case when the electric field is perpendicular to the magnetic field, the energy loss per unit volume due to joule heating can be expressed as $\mathbf{j} \cdot \mathbf{j}/\sigma_3$ ($= \mathbf{j} \cdot \mathbf{E}$), where

$$\sigma_3 = \sigma_1 + \frac{\sigma_2^2}{\sigma_1}$$

The effective conductivity σ_3 is called the *Cowling conductivity*. If the electric field is parallel to the magnetic field, the energy loss is $\mathbf{j} \cdot \mathbf{j}/\sigma_0$ as in the absence of the magnetic field. The Cowling conductivity plays an important role in the dynamo

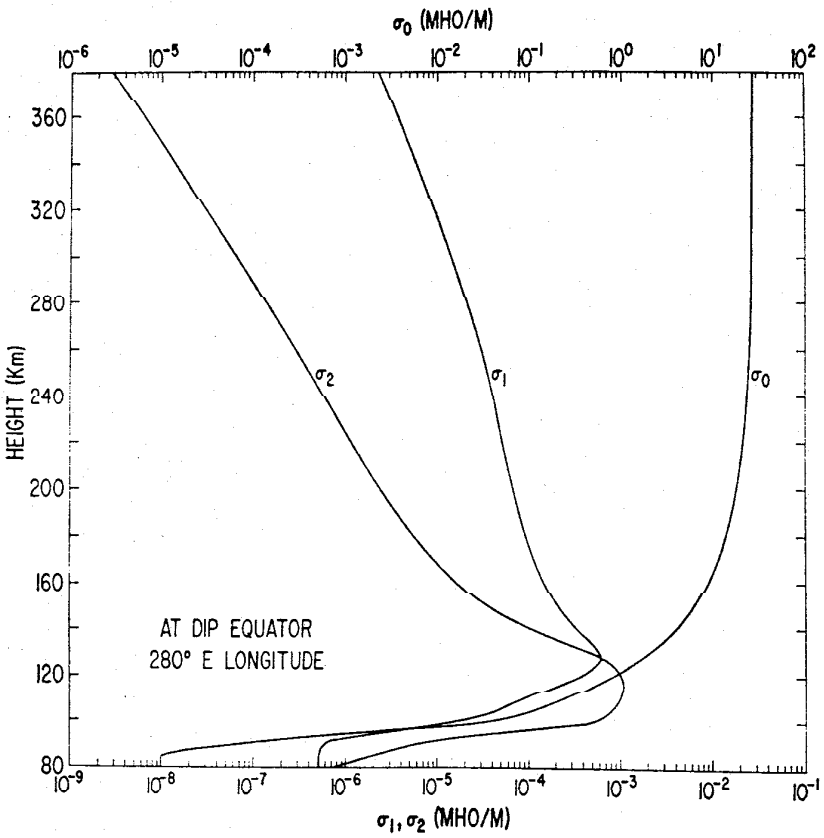

FIG. 5h-8. Typical conductivity profile (Sec. 5h-18); the upper scale for σ_0, the direct conductivity, and the lower scale for σ_1 and σ_2, the Pedersen and Hall conductivities, respectively.

region of the ionosphere. For instance, over the dip equator, where the magnetic field is horizontal, the effective conductivity for a horizontal electric field directed perpendicular to the magnetic field becomes σ_3 when the vertical Hall current is inhibited by polarization of the medium. The value of σ_3 is larger over the dip equator, and this is the reason for the existence of the equatorial electrojet mentioned in Sec. 5h-8.

The conductivities are latitude-dependent through the magnetic field, and also vary with the electron density distribution and hence with local time, latitude, season, and solar activity. The following rules generally hold: (1) The direct conductivity σ_0 is much larger than σ_1 and σ_2 throughout the ionosphere above about 70 km height; at this height σ_0 and σ_1 are approximately equal, indicating that the conductivity is nearly isotropic. (2) In the 90- to 130-km region, where the *Sq* (and *L*) current flows (Sec. 5h-8), σ_2 is larger than σ_1. (3) Above this region σ_1 becomes greater

than σ_2. Figure 5h-8 shows a typical conductivity profile for noon over the dip equator.

5h-19. Refractive Index in the Ionosphere [42]. For a plane electromagnetic wave propagating in a homogeneous magneto-ionic medium permeated by a uniform magnetic field, the complex refractive index n in the Appleton-Hartree approximation is given (in the standard notations and mks units) by

$$n^2 = 1 - \frac{X}{1 - iZ - \frac{1}{2}Y_T^2/(1 - X - iZ) \pm [\frac{1}{4}Y_T^4/(1 - X - iZ)^2 + Y_L^2]^{\frac{1}{2}}}$$

where $\omega_0^2 = Ne^2/\epsilon_0 m$
$\omega_H = \mu_0 H_0 |e|/m$
$\omega_L = (\mu_0 H_0 e/m) \cos\theta$
$\omega_T = (\mu_0 H_0 e/m) \sin\theta$
$X = \omega_0^2/\omega^2$
$Y_L = \omega_L/\omega$
$Y_T = \omega_T/\omega$
$Z = \nu/\omega$
ω = angular frequency of the wave
ϵ_0 = electric permittivity of free space
μ_0 = magnetic permittivity of free space
e = electron charge, numerically negative
m = electron mass
H_0 = magnitude of the ambient magnetic field $\mathbf{H}_0$
N = number density of electrons
θ = angle between $\mathbf{H}_0$ and the direction of propagation of the plane wave
ν = frequency of collision of electrons with heavy particles

The upper and lower signs in the above equation correspond to the *ordinary* and the *extraordinary* wave, respectively. For ionospheric propagation there are two useful approximations: the quasi-longitudinal (QL) and the quasi-transverse (QT) approximations.

For QL:
$$n^2 \doteq 1 - \frac{X}{1 - iZ \pm |Y_L|}$$

where the upper and lower signs are for the ordinary and the extraordinary wave, respectively.

For QT:
$$n^2 \doteq 1 - \frac{X}{1 - iZ + (1 - X - iZ)\cot^2\theta}$$

for the ordinary wave, and

$$n^2 \doteq 1 - \frac{X}{1 - iZ - Y_T^2/(1 - X - iZ)}$$

for the extraordinary wave.

These approximations are valid if the following conditions are satisfied:

$$\frac{Y_T^4}{4Y_L^2} \ll |(1 - X - iZ)^2| \qquad \text{for } QL$$

$$\frac{Y_T^4}{4Y_L^2} \gg |(1 - X - iZ)^2| \qquad \text{for } QT$$

The existence of the two modes, the ordinary and the extraordinary, is due to the presence of the magnetic field. In the absence of the latter the refractive index n would be given, ignoring the collision effects and the ion motions, by

$$n^2 = 1 - \frac{Ne^2}{\epsilon_0 m\omega^2}$$

A plane wave of angular frequency ω propagating vertically upward in a medium with electron density N varying with height will be reflected back at the height at which N reaches a value that makes n vanish; this value of N is given by

$$N = 1.24 \times 10^{-8} f^2$$

in terms of the wave frequency f ($= \omega/2\pi$) in hertz. Given N, the angular frequency ω_0 ($= \sqrt{Ne^2/\epsilon_0 m}$) is called the *electron plasma frequency.* If there is a peak in the electron density, say N_m, the plasma frequency is also a maximum, say ω_m, at the same height. Then radio waves with angular frequency ω less than ω_m will all be reflected from varying heights, and those with ω greater than ω_m will penetrate through the medium. The frequency f_m ($= \omega_m/2\pi$) is called the *critical* or *penetration* frequency of the medium. The electron collisions with heavy particles result in an absorption of the wave energy and a modification of the refractive index. In the ionosphere the latter modification is generally slight, and reflection still occurs near the level where the plasma frequency is equal to the wave frequency. The presence of the geomagnetic field introduces another complication, namely, that an incident wave is split into two waves, ordinary and extraordinary, with different polarizations, which propagate in general independently. The penetration frequencies for these two waves are different. For the ordinary wave this frequency is, under normal conditions, the maximum plasma frequency mentioned above.

MAGNETOSPHERE

5h-20. The Magnetic Field Configuration [2,43,44]. The earth's magnetic field is confined to a bounded region of space by the solar wind plasma (Sec. 5h-21); this region is called the *magnetosphere,* and its outer boundary, the *magnetopause.* Its inner boundary is not well-defined, but may be regarded as the altitude above which the convection of the plasma and the motion of the energetic charged particles are predominantly controlled by the geomagnetic field. If this altitude is taken to be that at which the cyclotron frequency of the main constituent ions becomes comparable with their collision frequency, this is about 150 km height or near the base of the ionospheric F region.

The magnetopause along the sun-earth line is at about $10R_e$($1R_e$ = earth's radius = 6371.2 km, Fig. 5h-9), and flares out toward its flanks to about $14R_e$ in the meridian plane through 6 and 18 hr local time [45,46]. Beyond about $20R_e$ behind the earth the magnetopause is nearly a cylindrical surface of radius 15 to $20R_e$, enclosing the *magnetosphere* tail [46]. The surface current on the magnetopause (which is a consequence of the solar wind particles being reflected away from the magnetopause) increases the magnetic field inside it; the effect of the current is such that the magnetic field intensity just inside the magnetopause is made approximately twice as large as it would be if there were no confinement of the field. Roughly speaking, the surface current flows from the morning to the evening side on the sunlit part of the magnetopause and closes its circuit by flowing around two foci, one in each hemisphere, so as to form two vortices around them. The magnetic field immediately inside the magnetopause is everywhere parallel to the magnetopause except directly behind the foci, where the magnetic field just inside is normal to the magnetopause. These two singular points are called the null pionts. The current on the nearly cylindrical part of the magnetopause enclosing the magnetosphere tail flows from the evening toward the morning side both on the northern and southern halves; how the current closes is not as yet understood, though there have been models in which the current returns to the evening side along the equatorial plane where the magnetic field is weak. The general picture depicted above is necessarily highly idealized and serves merely as a guide

toward a better understanding of the real magnetopause, which must have a much more complex structure.

The magnetic field configuration in the magnetosphere is schematically shown in Fig. 5h-10. Let the polar angle of the points at which the two magnetic field lines through the null points intersect the earth's surface be denoted by Θ_1, assuming, for simplicity, a symmetry with respect to the dipole equator. Then, Θ_1 is near 15° (i.e., near, but not necessarily always identified with, the poleward boundary of the auroral electrojet belt near noon, as shown in Fig. 5h-5) [47]. In the (geomagnetic) noon meridian half plane containing the null points, the field lines intersecting the

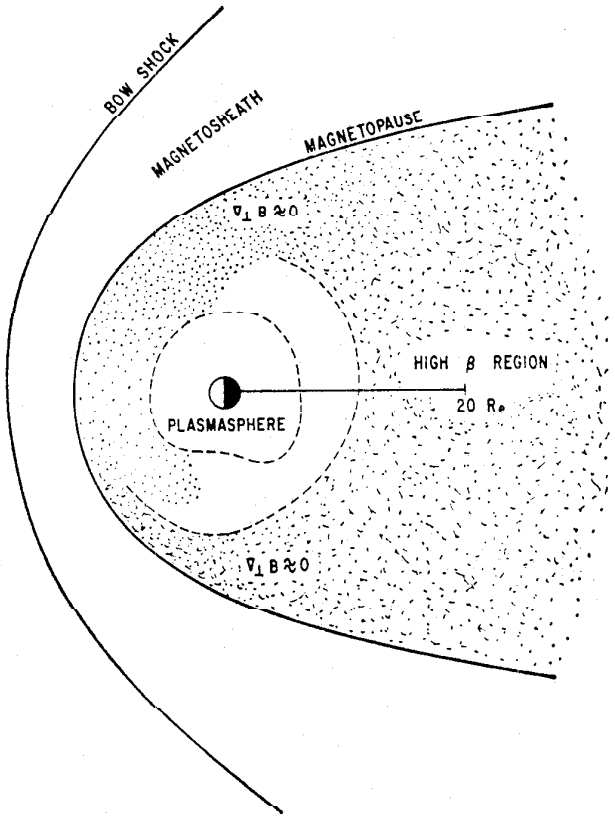

FIG. 5h-9. Illustrations of the magnetosphere (Secs. 5h-20 and 5h-21): equatorial cross section; dots represent presence of plasmas; the sun is to the left.

earth's surface at polar angles greater than Θ_1 are dipolar in their gross character, though they are deformed by the compression from the front. The field lines intersecting the earth's surface at polar angles less than Θ_1 are drawn back over the pole toward the tail. In the midnight meridian half plane all field lines extend toward the tail, but there is a somewhat analogous polar angle, say Θ_2, where the field lines leaving the earth at angles greater than Θ_2 maintain some characteristics of a dipolar field at large distances. This angle, Θ_2, is frequently near 19° and corresponds roughly to the poleward boundary of the auroral electrojet belt near midnight, as shown in Fig. 5h-5. The magnetic lines leaving the earth at polar angles less than Θ_2 extend to great distances in the geomagnetic tail (Fig. 5h-10) where they become nearly parallel to the direction of the solar wind flow outside the magnetosphere. The magnetospheric tail

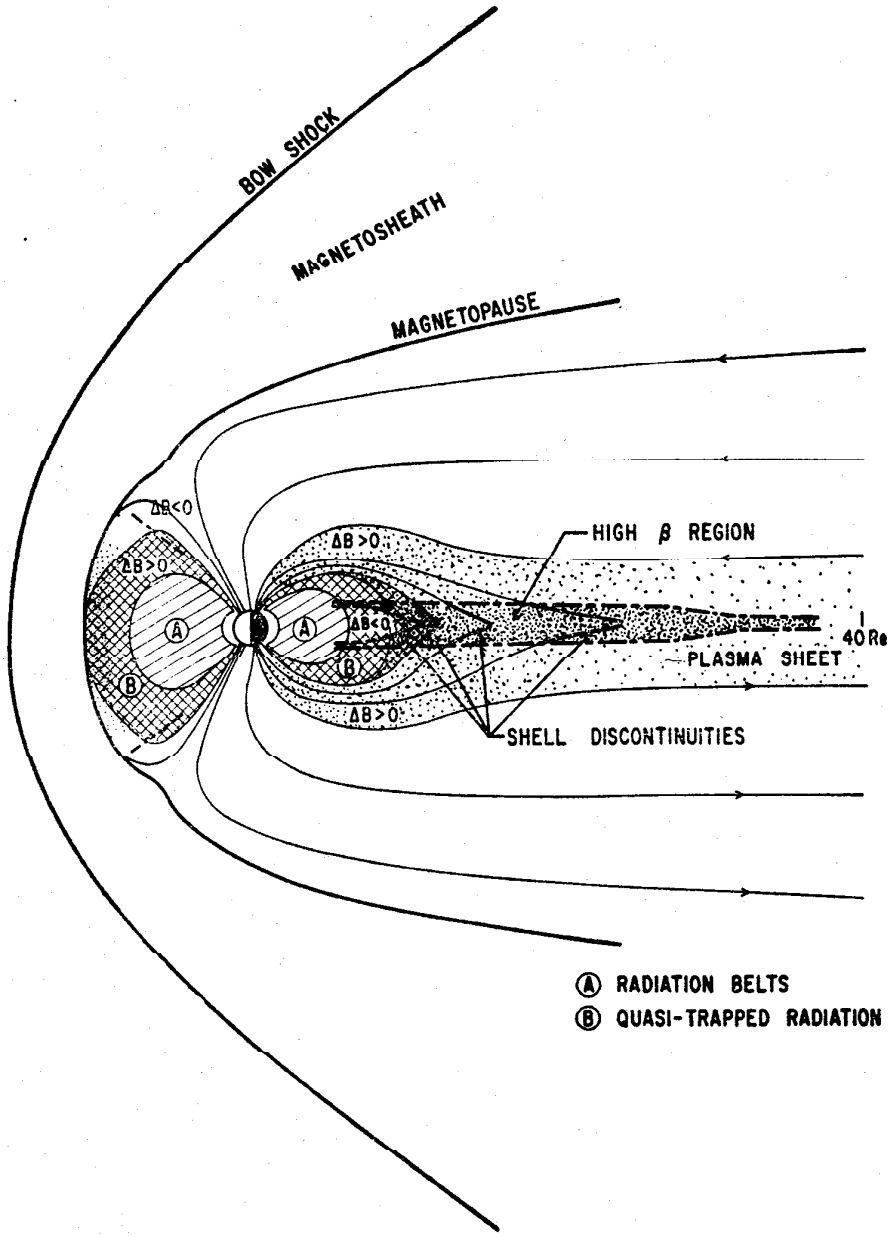

NOON-MIDNIGHT CROSS SECTION

FIG. 5h-10. Illustrations of the magnetosphere (Secs. 5h-20 and 5h-21): noon-midnight meridianal cross section; dots represent presence of plasmas; the sun is to the left, and the tail extends to the right.

extends to at least $80R_e$ [48] and may still exist at $1{,}000R_e$ in a less well-defined form [49,50]. In the midnight meridian a third polar angle, Θ_3, can be designated corresponding to the lowest latitude of the east-west auroral electrojet, shown schematically in Fig. 5h-5. The radiation belts (region *A* of Fig. 5h-10) lie on magnetic shells emanating from the earth at $\Theta > \Theta_3$. The magnetic field in the radiation-belt region is represented fairly accurately by the spherical harmonic description given in Sec. 5h-5. A transitory region (region *B* of Fig. 5h-10) where trapping of energetic (e.g., >40 kev) particles is highly variable usually bounds the outermost magnetic shell of

the radiation belts. Within the shells of this transitory region the spherical harmonic and dipole descriptions of the field become less accurate, and large deviations commonly occur. It has not been clearly established whether nightside field lines in region B (Fig. 5h-10) emanate from the earth at $\theta > \theta_3$ or $\theta < \theta_3$; θ_3 field lines could lie within region B or at the boundary between regions A and B. The uncertainty is greatly influenced by the fact that θ_3 (as noted in Sec. 5h-10) varies greatly with the level of activity. Close to the nightside equatorial plane beyond region B (Fig. 5h-10), in what can be called the *near-tail* region, the magnetic field maintains a shell-like structure, but is highly deformed by internal plasma pressures that inflate and stretch the field shells toward the antisolar direction. These shells emanate from the earth at $\theta_2 \leq \theta < \theta_3$.

For accurate mathematical description of the field in the outer magnetosphere expressions for the distortions created by the solar wind compression and the stresses exerted by plasmas within the magnetosphere and magnetospheric tail need to be added to the spherical harmonic description (Sec. 5h-5). However, as of 1970, expressions which adequately represent these effects analytically throughout the magnetosphere had not been derived. The time variability is one of the principal problems that is illustrated by considering some of the effects observed during storms, below, but present to some degree at all times: (1) a high solar wind pressure compresses the magnetosphere inward (Sec. 5h-12) such that θ_1 is increased and more magnetic flux is pushed back into the tail; (2) an enhanced plasma belt is created deep in the magnetosphere and exerts stresses that inflate the magnetosphere (Sec. 5h-11); (3) complex changes in the plasma behavior in the near-tail region locally disturb the field [51]; and (4) at the times of magnetic bays (Sec. 5h-10), or substorms, the plasma stress is partially released and the near-tail field suddenly relaxes, or collapses, toward a more dipolar configuration [45].

5h-21. Charged Particle Content. *Plasmas* [20,52,53]. The presence of plasmas in the magnetosphere and their influences on the magnetic field have been mentioned in Sec. 5h-20. High fluxes of plasma are observed in the *plasma sheet* that lies approximately on the equatorial plane separating the earthward magnetic field in the northern half of the tail from the oppositely directed field in the southern half (Fig. 5h-10). The thickness of the sheet is 4 to $6R_e$ at the distance from the earth of about $17R_e$. The electrons in the plasma sheet have a broad, quasi-thermal energy spectrum peaked anywhere between a few hundred and a few thousand electron volts with a non-Maxwellian high-energy tail. In the midnight sector the plasma sheet reaches, under quiet conditions, distances of about $10R_e$ from the earth and comes closer when disturbed. The sheet extends to the flanks and toward the front side, enveloping the magnetosphere, as shown in Figs. 5h-9 and 10. The inner boundary of the plasma sheet is well-defined on the evening to the afternoon side, but appears to be more diffuse on the morning side; however, detailed plasma behaviors on the dayside of the magnetosphere are as yet not known. On the nightside the plasma and the magnetic field show shell-like structures often with distinct discontinuities between neighboring shells. Whenever the ratio β of the plasma kinetic energy density ($\frac{1}{2}nmv^2$) to the magnetic field energy density ($B^2/8\pi$) exceeds unity, the magnetic field is disturbed by the diamagnetic effect of the plasma, and the dipolar characteristics of the field are appreciably modified or completely lost. An example of the latter is seen in the outer skirts of the magnetosphere near the dawn and dusk meridians and near the geomagnetic equator where the magnetic field gradient is almost zero from about $10R_e$ to the magnetopause.

From ground-based observations of whistlers (Sec. 5h-33) and direct satellite measurements, it has been found that sudden decreases in electron densities occur near the magnetic equatorial plane at distances from the earth's center that vary with local time and disturbance from 3.5 to $7R_e$. The region of higher electron densities, about

10^2 cm^{-3} is called the *plasmasphere*, as shown in Fig. 5h-9. The outer boundary of the plasmasphere is referred to as the *plasmapause*, and its position moves toward the earth during periods of high magnetic activity [54]. The plasmas inside the plasmasphere are of much lower energy than those in the plasma sheet, and unlike the latter, the plasma within the plasmapause is not known to play any major role in causing magnetic disturbances except that their presence makes the conductivity along the magnetic field lines very large.

Energetic Particles [19,55,56]. The magnetosphere is populated with charged particles of a wide range of energies. These particles are distinguished from such transients as galactic and solar cosmic rays by their being "trapped" in the geomagnetic field for varying lengths of time. Hence their motion in the geomagnetic field is of fundamental importance; basic properties of their motion are discussed in Sec. 5h-22. Energies of the plasmas discussed above partially overlap with the low-energy part of particles described here, and the division of the charged-particle content of the magnetosphere into plasmas and energetic particles becomes arbitrary in some cases. Grouping of the particle populations is not definitively settled and is subject to future revisions. However, roughly speaking, the energetic particles in the magnetosphere can be divided into two groups: *trapped* and *quasi-trapped* particles. The definition of "being trapped" is by no means unambiguous; if a particle drifts around the earth repeatedly, it is considered to be trapped; see Sec. 5h-22 for particle drifts.

The region of trapped particles is from $L \sim 1.2$ to 6; see Sec. 5h-22 for the definition of L. This population includes the so-called inner and outer radiation zones or belts that were discovered by the early probes. The inner zone contains protons of energies, $E > 30$ Mev, with fluxes of about 10^4 cm^{-2} sec^{-1}, and peak intensities near $L \sim 1.5$; these particles are relatively stable with a time constant of the order of 1 year. The outer zone with electrons of $E > 1.5$ Mev is at $L \sim 3$ to 4, and its flux is highly variable, particularly during magnetic storms. The time constant for these electrons is roughly hours to weeks. These early observations of penetrating radiation with heavily shielded Geiger tubes led to the concept of the inner- and outer-zone structure with a "slot" near $L \sim 2$ where the count rate was a minimum [57]. However, later observations of particles in wider energy ranges have revealed that the structure described above was, to some extent, due to instrumental factors, and that different group of particles have grossly different spatial distributions and time variations, some with double peaks and a minimum near $L \sim 2$, and others without such a structure. Nevertheless the terms "inner and outer zones" are used to refer to the regions approximately $L < 2$ and $L > 2$, respectively, without implying that the two regions are separated by a sharply defined boundary. Protons in the energy range 0.1 Mev $< E < 5$ Mev occupy the outer zone from $L \sim 2$ to 6 and are found to be relatively stable with small fluctuations on time scales of days; this population of protons has high fluxes with a peak of the order of 10^8 cm^{-2} sec^{-1} near $L \sim 3.5$ and carries most of the energy content of the trapped particles. Low-energy protons of E from a few kev to about 50 kev occupy a broad region from 3 to $10R_e$, and their fluxes vary greatly during magnetic storms. These low-energy protons are mainly responsible for the inflation of the magnetosphere and the *Dst* decrease on the earth's surface during magnetic storms, described in Sec. 5h-11. The contribution to the storm effects from electrons in the energy range from a few hundred ev to 50 kev is likely to be appreciable, but probably only about one-fourth of that from the protons [20]. Electrons with higher energies (e.g., $E \gtrsim 300$ kev) occupy the outer zone, and their fluxes suddenly increase at the time of magnetic storms and decay to an equilibrium level with a time constant of days to weeks [58,59]. The sources of the trapped particles are not as yet well understood. The radioactive decay of albedo neutrons produced by nuclear collisions of galactic (and solar) cosmic-ray protons with oxygen and nitrogen nuclei in the atmosphere has been proposed to be the main source for the high-energy protons

in the inner zone. For the outer-zone protons, several processes involving an inward diffusion and acceleration have been proposed; but there are no definitive proofs as to how efficient these mechanisms are. One suggestion is that the diffusion is caused by violation of the third adiabatic invariant (Sec. 5h-22), due to such magnetic perturbations as sudden impulses (Sec. 5h-12), and that conservation of the first and second invariants (Sec. 5h-22) leads to energization of the particles as they diffuse inward. A similar process resulting from fluctuations in the electric field of the magnetospheric convection system (Sec. 5h-23) has also been considered.

The series of high-altitude nuclear explosions of 1958 (i.e., the Argus experiment) was designed to test the possibility of trapping energetic particles by the geomagnetic field [60]. Electrons mainly from the β decay of the fission fragments were injected into a thin shell near $L \sim 2$, and were found to be stable in position during their lifetime of a few weeks. The Starfish explosion of July 9, 1962 [61] created a more intense and extensive artificial radiation belt; initially, a maximum flux ($\sim 10^9$ electrons cm^{-2} sec^{-1}) was near $L \sim 1.3$ with large fluxes extending to beyond $L \sim 4$. For $L < 1.5$ the electron decay was slow, with lifetimes of the order of years, and was in agreement with the theoretical expectation for decay from Coulomb scattering of the electrons in the atmosphere. Beyond $L \sim 1.7$ the decay was considerably faster, with lifetimes of months to a week; the rapid decay was thought to be due to resonant interaction of electrons with electromagnetic waves such as whistlers (Sec. 5h-33) or due to processes related to magnetic disturbances. Interactions between particles and electromagnetic waves of various frequencies from VLF to ELF or ULF (Secs. 5h-29 to 5h-33) constitute an important subject concerning the particle behaviors in the magnetosphere [62], but direct observational evidence for these interactions is in most cases still lacking.

The quasi-trapped particles occupy regions between the trapping region and the magnetopause on the front to the flanks of the magnetosphere, and the near-earth tail region on the nightside. These particles mainly consist of low-energy protons and electrons with $E \lesssim 50$ kev. Their fluxes are highly variable with geomagnetic activity; this population and its extension into the near-tail plasma sheet is probably the reservoir for the particles precipitating into the atmosphere during high-latitude disturbances. A major supply of particles for the trapping region may also come from the quasi-trapping region. Occasional high fluxes of particles have been observed in different regions: for instance, sudden flux increases of electrons with $E \gtrsim 40$ kev and with omnidirectional fluxes up to about 10^7 electrons cm^{-2} sec^{-1} observed in the tail [63] (often referred to as electron "islands") and "spikes" of directional electron fluxes up to 10^9 electrons cm^{-2} sec^{-1} $sterad^{-1}$ encountered at low altitudes ($\sim$1,000 km) [64] are examples of intensified particle activity in the quasi-trapping region.

5h-22. Energetic Particle Motion [2,56,65,66]. There are three fundamental characteristics in the motion of a charged particle in a dipole-type magnetic field such as the earth's field: (1) gyration about a line of force, (2) oscillation between mirror points along lines of force, and (3) longitudinal drift around the center of the dipole. Corresponding to these three periodicities there are three *adiabatic invariants* that are conserved.

For the gyrating motion the *first*, or *magnetic moment, invariant* μ is given by

$$\mu = \frac{P_\perp{}^2}{2m_0 B}$$

where $P_\perp$ = the component of the (relativistic) momentum perpendicular to the magnetic field vector **B**
m_0 = the particle rest mass
B = $|\mathbf{B}|$

The motion of a charged particle can be investigated with high accuracies by an approximation in which the center of the gyrating motion, referred to as the *guiding center*, is followed. For the oscillatory motion of the guiding center between mirror points, the *second*, or *longitudinal, invariant* is conserved. This invariant, J, is defined by

$$J = \oint P_{\parallel}\, ds$$

where $P_{\parallel}$ is the guiding-center momentum parallel to the line of force, and the integral is taken over a complete oscillation. For J to be conserved, the drift velocity perpendicular to the lines of force along which the guiding center oscillates must be small compared with its velocity along the line of force.

The guiding center drifts from a line of force to an adjacent line of force such that J is constant, and thus the lines of force, along which the guiding center moves, form a surface on which J is constant. If this surface is closed, namely, if the guiding-center returns to a line of force which it previously traversed, there is a third periodicity. For this precessional motion of the guiding center, the *third*, or *flux, invariant* is conserved. The invariant is the magnetic flux Φ, enclosed by the closed surface just described. Obviously, if the magnetic field is static, this invariant is trivial, but it remains constant even when the field varies in time, provided that the time of precession is small compared with the time scale for the field variations. Thus the third invariant Φ is the first to be violated when the time scale of field fluctuations becomes short; the next is the second invariant J; and the first invariant μ is violated only by very rapid field variations with periods less than the particle's gyroperiod.

From the constancy of μ, the relation between the magnetic field strength B and the *pitch angle* α (= the angle between the velocity vector and the line of force about which the particle gyrates) is

$$\frac{\sin^2 \alpha}{B} = \text{constant}$$

In particular, if $B = B_m$ at the mirror point (where $\alpha = \pi/2$), the pitch angle at the equator α_0 is given by

$$\sin \alpha_0 = \left(\frac{B_0}{B_m}\right)^{\frac{1}{2}}$$

where B_0 is B at the equator.

If μ is constant, and if there is no electric field,

$$J = 2P \int_A^{A'} \left(1 - \frac{B}{B_m}\right)^{\frac{1}{2}} ds$$

where P is the linear momentum, and the integral is taken over a half oscillation from one mirror point A to its conjugate point A'. The quantity I defined by

$$I = \frac{J}{2P}$$

is a function of the mirror point A and the magnetic field configuration, and is independent of the particle properties. I can be considered as a function of position only, if the mirror point A is taken to be coincident with the point for which I is being evaluated. For a dipole field of moment M the quantity $L_d{}^3B/M$ can be expressed as a function, say F, with an argument I^3B/M,

$$\frac{L_d{}^3B}{M} = F\left(\frac{I^3B}{M}\right)$$

where L_d is the distance from the dipole to the equatorial crossing of the line of force that passes the point at which I is being evaluated. For the earth's magnetic field the *magnetic shell parameter* [67], L, is defined by the formula

$$\frac{L^3B}{M} = F\left(\frac{I^3B}{M}\right)$$

where the functional form of F is taken to be identical with the corresponding function for the dipole field, but B and I are now computed using the spherical harmonic expression as given in Sec. 5h-5; M is the earth's magnetic dipole moment. L is usually measured in units of earth radii. Data for the trapped particles are normally organized in the (B,L) coordinate system. Because of the distortions of the geomagnetic field by the solar wind (Sec. 5h-20) and the charged particles inside the magnetosphere (Sec. 5h-21), the B, L coordinates as computed from the spherical harmonic expression for the surface field are usually accurate only to $L \sim 5$. Beyond this distance the B, L coordinates computed in this way become gradually meaningless with increasing distance. At present there is no adequate analytical expression for the distorted magnetosphere field.

So far the motion of a charged particle has been considered in the presence of a magnetic field **B**. In the presence of an electric field **E** in addition to **B**, the particle drifts in a direction transverse to **B** with a velocity $\mathbf{v}_t$ given in a guiding-center approximation by

$$\mathbf{v}_t = \mathbf{E} \times \frac{\mathbf{B}}{B^2} + \epsilon_\perp \mathbf{B} \times \frac{\nabla B}{qB^3} + 2\epsilon_\parallel \mathbf{B} \times \frac{\mathbf{R}}{qB^2R^2}$$

where $\epsilon_\perp$ and $\epsilon_\parallel$ are kinetic energy perpendicular and parallel to **B**, respectively; q is the charge; **R** is the vector radius of curvature of the field line about which the particle gyrates: $R = |\mathbf{R}|$, and in the absence of currents, $1/R = \nabla_\perp B/B$. The three terms are often referred to as the $\mathbf{E} \times \mathbf{B}$ drift, the gradient drift, and the curvature drift, respectively. The longitudinal drift mentioned earlier corresponds to the combined effects of the gradient and curvature drifts in the geomagnetic field.

5h-23. Plasma Convection [2,68]. If a plasma in a magnetic field is taken to be a perfect conductor, Ohm's law is expressed by

$$\mathbf{E} + \mathbf{v} \times \mathbf{B} = 0$$

where **E** and **B** are the electric and magnetic field intensities, respectively, and **v** is the bulk velocity of the plasma. Under these conditions the magnetic field is referred to as a *frozen-in* field [66,69,70], and magnetic field lines can be identified by the plasma. $\mathbf{E} + \mathbf{v} \times \mathbf{B} = 0$ is also referred to as the *hydromagnetic approximation*, and as an approximation it has been useful in explaining the generation of electric fields in the magnetosphere and the consequences of these electric fields in causing electric currents in the ionosphere and electric field drifts (Sec. 5h-22) (proportional to $\mathbf{E} \times \mathbf{B}/B^2$) of energetic particles (i.e., particles of higher energy in populations of lower-energy density than the plasma particles moving in bulk with velocity **v**). In the frozen-in state, motions of plasma and magnetic field lines leave the magnetic field configuration unchanged and are said to interchange the lines of force. This has led to the concept that there may be a continuous convection of plasma in the magnetosphere. The geomagnetic field lines are also tightly "frozen" into the earth because of its high conductivity; however, the presence of a nonconducting neutral atmosphere between the earth and the ionosphere decouples the two frozen-in regions and makes magnetospheric *interchange motions* [71] possible. If the magnetic field configuration is unchanged, $\partial\mathbf{B}/\partial t = 0$, and consequently curl $\mathbf{E}$ = curl $(-\mathbf{v} \times \mathbf{B}) = 0$.

This implies that magnetic lines of force and the streamlines of the flow are equipotentials of the electric field. Also, because magnetospheric magnetic fields are not uniform, interchange motions are accompanied by changes in plasma density and by adiabatic heating and cooling of the plasma during compressions and expansions.

The gross pattern of convection in the magnetosphere and magnetospheric tail has been largely inferred from the distribution of currents associated with the auroral electrojets (Sec. 5h-10), using two assumptions: (1) that the Hall conductivity σ_2 is much greater than the Pedersen conductivity σ_1 in the lower ionosphere (Sec. 5h-18), and (2) that the magnetic field lines in and above the lower ionosphere are lines of infinite conductivity and thus equipotential lines [47,72–74]. The electric field $\mathbf{E} = -\mathbf{v} \times \mathbf{B}$ perpendicular to the electric current in the direction $-\mathbf{v}$ (i.e., opposite $\mathbf{v}$ as a consequence of the electron motion in the region 100 to 130 km where the ion's transverse motion is inhibited by collisions) then maps directly into the magnetosphere from hemisphere to hemisphere. In the magnetospheric equatorial plane this produces a flow pattern in which plasma adjacent to the magnetopause on the nightside and near the twilight meridians flows, in general, away from the sun, and plasma in the central regions of the near-earth tail flows toward the sun. This picture is frequently interpreted as indicating that viscous interaction between the solar wind and magnetosphere pushes the outermost magnetospheric field and plasma roughly parallel to the direction of the solar wind flow. The flow from the tail toward the earth and sun is then regarded as the return flow. There are substantial reasons for believing that some such convection pattern exists associated with the auroral electrojects. In detail, however, the hydromagnetic approximation cannot strictly hold in that the ionospheric Pedersen conductivity is not negligible and tends to short-circuit the convective electric field. Deviations from the hydromagnetic approximation involving electrical loading in the ionosphere may, in fact, be responsible for many of the dynamical changes (e.g., the collapse of the near-tail magnetic field with the onset of a magnetic bay (Sec. 5h-20) can be viewed as being caused by an ionospheric release of the plasma pressure in the distant magnetosphere).

Other effects, in addition to Pedersen current short circuiting, can cause a breakdown of the hydromagnetic approximation. Lack of sufficient plasma density to justify the infinite conductivity assumption is one possibility that could be important along the polar cap field lines extending deep into the magnetospheric tail. The hydromagnetic approximation also loses validity in regions where the electron and ion pressures are large; in these cases the expression becomes $\mathbf{E} + \mathbf{v} \times \mathbf{B} = (ne)^{-1} \operatorname{grad} p$, where n, e, and p are the number density, charge, and pressure. Thus, in association with field shell discontinuities (Sec. 5h-20) in the near-tail and other large irregularities, significant deviations from the approximation are expected. Many outstanding problems in magnetospheric dynamics are closely related to determining the degree of applicability of the hydromagnetic approximation. Inasmuch as the problems relate to having information on electric fields in space, additional discussion is given in Sec. 5h-28.

INTERPLANETARY MEDIUM

5h-24. The Solar Winds [43,44,75,76]. One of the basic dynamical properties of the solar corona is its continuous expansion outward. The resulting plasma flow is referred to as the *solar wind*. The solar wind velocity varies with activity on the sun, and ranges from 300 to about 850 km sec^{-1}. The azimuthal direction of the average flow of the ions is 2 or 3 deg east of the sun after aberration due to the earth's orbital motion is corrected for, but the deviations in the arrival angle from the above average can be as large as 15 deg. Deviations of the flow direction from the solar ecliptic plane by as much as 5 deg have also been observed. Statistically the daily mean

solar wind velocity v is related to the daily sum of three-hourly geomagnetic activity index K_p (Sec. 5h-13) by a formula [77]

$$v \text{ km sec}^{-1} = 8.44\Sigma Kp + 330$$

However, on a finer time scale geomagnetic activity is not related to the solar wind velocity in any simple manner. The solar wind gas is mainly composed of electrons and protons. It also contains alpha particles in considerably variable quantity, from less than 1 to nearly 20 percent, with an average of 3 to 6 percent. A typical ion density in the solar wind is 1 to 10 protons cm^{-3}, but low values of less than 0.1 proton cm^{-3} and a maximum exceeding 80 protons cm^{-3} have been observed. A transverse "temperature" (for the direction normal to the bulk velocity) has been determined from the angular distribution of the ion velocities. The proton temperature so defined varies from 10^4 to 10^6 K. The temperature determined for the direction parallel to the bulk velocity appears to be greater than the transverse temperature by a factor typically about 5 [78]. Data on the electron temperature in the solar wind are scarce, but a characteristic temperature of 8×10^5 K has been reported for low-energy electrons in the energy range between 33 and 1,000 ev; however, the electron temperature is likely to change appreciably with solar activity, as does the bulk velocity of the ions [79].

5h-25. Interplanetary Magnetic Field [43,44,75,80]. Solar magnetic fields that extend beyond the solar corona are swept outward into interplanetary space by the solar wind (Sec. 5h-24). Thus, interplanetary space is permeated by magnetic fields of solar origin to distances that are thought to be of the order 100 AU (1 AU = mean sun-earth distance, $1.496 \cdot 10^{13}$ cm). The intensity of the interplanetary magnetic field near the earth's orbit is usually within the range 2 to 10 γ, with an average near 5 γ [81], but values as high as 25 γ are occasionally encountered. Although highly variable in direction, the statistical average direction in the ecliptic plane is closely approximated, considering only the rotation of the sun and the solar wind velocity. Thus, taking α as the angle between a radial line from the sun and the magnetic field in the ecliptic plane: $\alpha = \tan^{-1}(\omega r/v) = \tan^{-1}(428/v)$ at 1 AU where r = distance from the sun, ω = angular velocity of the sun's rotation, and v = solar wind velocity in km sec^{-1}.

In the ecliptic plane the magnetic field pattern sometimes indicates a sector structure with the field direction alternately pointing toward or away from the sun (on an average at angle α) in neighboring sectors. This pattern then corotates with the sun at its rotational period of approximately 27 days [81]. Although the magnetic field is clearly dominated by the solar wind, in that its energy density is only of the order of 1 percent of the kinetic energy density of the solar wind, it significantly modulates the flux of solar cosmic rays whose energy density is considerably less than that of the field. The flux of solar cosmic rays is thus anisotropic and roughly follows the filamentary magnetic flux tubes that constitute the prominent fine structure of the field [82]. In addition to this fine structure, hydromagnetic discontinuities are caused by the transient and nonuniform emission of solar wind plasma from the sun. These discontinuities develop into shock waves or form stationary contact surfaces, in the frame of reference of the plasma [83]. Effects of interplanetary discontinuities on the magnetosphere are discussed in Sec. 5h-26.

5h-26. Solar Wind–Magnetosphere Interaction [2,44]. The Alfvén speed v_A (Sec. 5h-29) in the solar wind is typically 60 km sec^{-1} (with density n = 3 protons cm^{-3}, and B = 5 γ); and hence the solar wind is hydromagnetically supersonic with a representative Alfvén Mach number, $M_A (= v/v_A)$, of 7. Because of the variability in n and B, M_A may be as low as 1.5 or may exceed 10. A standing bow shock is created on the upstream side of the magnetosphere boundary (Sec. 5h-20), analogous to that

of an object placed in a supersonic flow of fluid. Whereas in the latter case sound waves communicate the presence of the object upstream to divert the flow around it, magnetoacoustic waves, which have a group velocity of the order of the Alfvén speed, convey the message upstream in the solar wind to the shock. Since the mean free path in the interplanetary medium is of the order of 1 AU, the magnetosphere bow shock is a collision-free shock.

In the subsolar region the flow is subsonic behind the shock with ion velocities considerably randomized. As the gas flows toward the flanks of the magnetosphere, the flow becomes more ordered, and beyond a sonic line the velocity is again supersonic. The flow pattern appears to be in agreement with theoretical results obtained using continuum models for the solar wind.

According to gasdynamical calculations, the distance D from the earth's center to the magnetosphere boundary along the sun-earth line is approximately given by [84]

$$D = aH_0^{\frac{1}{3}}(2\pi K\rho v^2)^{-\frac{1}{6}}$$

where a = earth's radius = 6.3712×10^8 cm
H_0 = dipole field intensity on earth's surface at the equator = 0.30953 gauss
ρ = solar wind density
v = solar wind velocity
K = an adjustable constant which depends on the ratio of the specific heats, $\gamma(= C_p/C_v)$

For large Mach numbers K approaches 0.844 for $\gamma = 2$ and 0.881 for $\gamma = \frac{5}{3}$. For a Newtonian gas model K is 2 if the particle reflection at the boundary is assumed to be specular or "elastic," or unity if this is assumed to be "inelastic." For large Mach numbers the standoff distance Δ at the nose of the magnetosphere can be expressed approximately by [84]

$$\frac{\Delta}{D} = \frac{1.1[(\gamma - 1)M_A^2 + 2]}{(\gamma + 1)M_A^2}$$

These theoretical results roughly agree with observations [45]. Representative observational values of D and Δ are 10 and 3 earth radii, respectively. As a result of the solar wind–magnetosphere interaction, the earth's magnetic field is drawn out to large distances forming a magnetosphere tail (Sec. 5h-20).

ELECTRIC FIELDS

5h-27. Atmospheric Electricity [85,86]. Electrical phenomena between the earth's surface and an altitude of 30 km (roughly the peak altitude for airplane and balloon observations) are usually referred to as being atmospheric. At altitudes >80 km, measurements of "electric fields in space" (Sec. 5h-28) have only recently been initiated. Between 30 and 80 km, measurements are essentially nonexistent, and theory is at most only an extrapolation from the lower "atmospheric" regions.

Within the atmospheric region the ionizing agents are primarily cosmic rays and radiation from radioactive material in the earth and dust (both natural and from bomb debris). The vertical atmospheric electric field under clear weather conditions decreases rapidly with altitude from roughly 100 to 200 volts meter^{-1} at the surface to 10 to 30 volts meter^{-1} at an altitude of 6 km. Above roughly 10 km the potential gradient is often too weak to measure reliably, but appears typically to decrease to about 5 and 1 volts meter^{-1}, at 10 and 20 km, respectively. The conductivity (which depends primarily on ion mobilities) increases over these altitudes and ranges roughly from 1 to 10 to 30 $\times 10^{-14}$ ohm^{-1} meter^{-1} at 0, 6, and 10 km, respectively. Field intensity and conductivity values, such as those above, are subject to many

variations, even under clear weather conditions. Both seasonal and diurnal variations are generally recognized. Secular changes are also reported, which appear to be related to artificial factors such as changes in air pollution and periods of bomb testing. The fair weather electric field is negative upward such that positive ions move toward the earth. This fair weather electric current is, in general, considered to be a return current in that the principal generators for air-earth currents lie in regions where the atmosphere is disturbed by thunderstorms and precipitation. Models of the electrical structure of thunderstorms have been constructed for particular cases, but there is little agreement on the generality of such models when lightning and precipitation are included. Electric fields of several thousand volts per meter are commonly associated with disturbed conditions. The total potential drop associated with lightning reaches values of several million volts.

5h-28. Electric Fields in Space [14,19]. Direct space measurements of the electric field **E** have only recently become feasible by measuring differences in floating potential between identical probes, symmetrically oriented relative to the spacecraft motion and the sun, and separated by long base lines for each axis of measurement [87]. The measurements have been successfully conducted in the ionosphere between 80 and 300 km at middle latitudes and in the auroral belt. Measurements have also been attempted in traverses through the magnetosphere and into the interplanetary medium, but these, to date, have involved errors, due to insufficient base line relative to plasma sheath phenomena, that prohibit accurate d-c values. Limits on the electric field and valid a-c electric field measurements (Secs. 5h-32 and 5h-33) have, however, come from these early efforts. Electric fields have also been indirectly measured by observing the motion of artificially created barium ion clouds above the region (approximately below 180 km) where collisions affect the cloud motion. The motion **v** in the known magnetic field **B** gives the electric field **E** from $\mathbf{E} + \mathbf{v} \times \mathbf{B} = 0$ (Sec. 5h-23) [88].

The principal source of electric fields in the outer magnetosphere and high-latitude ionosphere appears to be the convection of plasma (Sec. 5h-23) driven indirectly by interaction between the solar wind and the earth's magnetic field. Both direct probe measurements [89] of **E** and motion measurements of **v** for artificial Ba^+ clouds [90] have demonstrated that auroral electrojet currents are mainly Hall currents (in the direction $-\mathbf{v}$ as shown by the simultaneous magnetic disturbance field of the current) in that the quantities **v** and **E** have both been found to be at right angles to **B** in a number of cases, including examples of both eastward and westward electrojet flow (Fig. 5h-5). These measurements essentially show that the hydromagnetic approximation (Sec. 5h-23) $\mathbf{E} + \mathbf{v} \times \mathbf{B} = 0$ gives a reasonable picture of the convection dynamics in the auroral belt (Sec. 5h-10) region. The lack of a **v** component along **B** and one example [89] of a constant value for **E** between roughly 90 and 130 km when a probe trajectory fell along a magnetic field line during that section of a rocket flight provide additional support for treating the magnetic field lines as equipotentials. However, while verifying the proper vector relationships for $\mathbf{E} + \mathbf{v} \times \mathbf{B} = 0$ the measurements have shown that the electric field is highly variable in magnitude and can drop to extremely low values in narrow shells where the ionospheric conductivity is exceptionally high. These narrow shells contain discrete auroral forms. Over most of the belt within which aurora is occurring **E** is found to be > 0.01 volt meter^{-1} with values between 0.02 and 0.05 volt meter^{-1} being fairly common [89,90]. Values as high as 0.13 volt meter^{-1} have been observed, and as the total time of sampling has been small, it is highly probable that greater intensities are not uncommon. In contrast, directly on shells of discrete auroral forms **E** has been observed to drop below 0.005 volt meter^{-1}, which suggests that the **E** field is partially short-circuited in local strips of exceptionally high ionospheric conductivity. Observations that visual auroral structures show identical details when observed simultaneously at

conjugate points in the northern and southern auroral belts [91] and that the magnetic disturbances are correlated in detail [92] illustrate that the potential distribution maps from hemisphere to hemisphere along magnetic field lines. Corresponding field intensities in the equatorial plane of the magnetosphere, taking into account the magnetic field geometry and its distortion in the near-tail region, are roughly 20 to 100 times less than in the ionosphere along the same magnetic shells.

Over the polar cap (Sec. 5h-10) there have not been definitive electric field measurements. If the polar-cap ionospheric currents are Hall currents, it can be estimated that the electric field has properties similar to those observed in the auroral belt. It is also not known whether or not magnetic field lines emanating from the polar cap can be treated as electrical equipotential lines in that plasma densities at large distances along these shells outside the equatorial plasma sheet in the tail have been below measurement thresholds.

In middle- and low-latitude regions **E** and **v** measurements in and above the ionosphere have given values in the range 10^{-4} to 2×10^{-3} volt meter^{-1}, which in most cases is close to the magnitude of possible errors in measurement [88–90]. Measurements have not been made during periods of large disturbances, or storms, when one might expect the high-latitude convection system to penetrate more deeply into the magnetosphere. **E** magnitudes of the order 10^{-3} volt meter^{-1} can be expected from the *Sq* (Sec. 5h-8) dynamo (i.e., winds) in the ionospheric E region [93].

In addition to the convection process, a variety of mechanisms have been proposed for generating electrostatic fields relevant to specific problems in the ionosphere and magnetosphere [74,94,95]. Other than those cases where the indirect evidence is convincing (e.g., the polarization field required for the equatorial electrojet, Sec. 5h-8), their existence and/or importance is unproved. Electrostatic electric fields also play an essential role in a number of theoretical treatments of the magnetopause boundary and the bow shock (Sec. 5h-26). In the case of the bow shock, fields as strong as 5 volts meter^{-1} have been postulated as existing in a thin region at the shock front [96]. However, the limited measurements available indicate that the fields are more of the order $-\mathbf{v} \times \mathbf{B}$, where **v** is the plasma bulk velocity as in the hydromagnetic approximation (Sec. 5h-23) [89]. Similarly, in the interplanetary medium, **E**, as indicated in the spacecraft frame of reference, is compatible with $-\mathbf{v} \times \mathbf{B}$ for the solar wind velocity **v** (*Note.* This field does not exist in the frame of reference of the solar wind which is moving with velocity **v**.) For typical ranges of solar wind–interplanetary magnetic field parameters, the range of **E** (in spacecraft coordinates) is roughly 10^{-3} to 10^{-2} volt meter^{-1} [89].

Relative to accelerating charged particles that enter the earth's (magnetospheric) frame of reference from inertial space, an additional electric field exists which is caused by charge separation induced by the rotation of the ionosphere with the earth [72,73]. The potential of this *corotational* field in the ionosphere is $V = 90 \sin^2 \Theta$ in kilovolts, where Θ is the colatitude. As the corotational field is zero in the earth's reference frame, it does not create currents.

WAVE PHENOMENA

5h-29. Magnetohydrodynamic Waves [66,69,97]. *Alfvén Waves.* In a perfectly conducting fluid permeated by a uniform magnetic field $\mathbf{B}_0$, Alfvén waves propagate in the direction of $\mathbf{B}_0$ with the Alfvén velocity V_A given by

$$V_A = \frac{B_0}{\sqrt{4\pi\rho}}$$

where $B_0 = |\mathbf{B}_0|$ (in emu, i.e., in gauss) and ρ = density (in cgs units, i.e., g cm^{-3}). The magnetic perturbation **b** and the fluid velocity **v** are both transverse to $\mathbf{B}_0$; and $b^2/8\pi = \frac{1}{2}\rho v^2$; i.e., an equipartition of energy holds.

Magnetoacoustic Waves. In a perfectly conducting, compressible fluid permeated by a uniform magnetic field $\mathbf{B}_0$, magnetohydrodynamic waves propagate with a phase velocity V that satisfies

$$V^4 + (V_A^2 + C_0^2)V^2 + V^2C_0^2 \cos^2\theta = 0$$

where V_A = Alfvén velocity ($= B_0/\sqrt{4\pi\rho}$)
C_0 = sound velocity ($= \sqrt{\gamma p/\rho}$; γ = ratio of specific heats, p = pressure, and ρ = density)
θ = angle between $\mathbf{B}_0$ and direction of propagation

When $\theta = 0$, the roots of the above equation are $\pm C_0$ and $\pm V_A$, corresponding to a pure acoustic wave and a pure Alfvén wave propagation along $\mathbf{B}_0$. When $\theta = \pi/2$, there is only one mode propagating with phase velocity, $V = \pm(C_0^2 + V_A^2)^{\frac{1}{2}}$; in this wave the fluid velocity $\mathbf{v}$ is perpendicular to $\mathbf{B}_0$, and the magnetic perturbation $\mathbf{b}$ is parallel to $\mathbf{B}_0$. The latter velocity is called the *magnetoacoustic* velocity. Between $\theta = 0$ and $\pi/2$ the two modes are coupled.

5h-30. Plasma Waves [98,99]. *General.* For a two-component (electron-ion) cold plasma in a uniform magnetic field B_0 the dispersion equation is given by

$$An^4 - Bn^2 + C = 0$$

where n = refractive index ($= |\mathbf{k}|c/\omega$; $\mathbf{k}$ = angular wave number, c = velocity of light)

$$A = S\sin^2\theta + P\cos^2\theta$$
$$B = RL\sin^2\theta + PS(1 + \cos^2\theta)$$
$$C = PRL$$
$$S = \tfrac{1}{2}(R + L)$$
$$D = \tfrac{1}{2}(R - L)$$
$$R = 1 - \alpha\omega^2/[(\omega + \Omega_i)(\omega - \Omega_e)]$$
$$L = 1 - \alpha\omega^2/[(\omega - \Omega_i)(\omega + \Omega_e)]$$
$$P = 1 - \alpha$$
$$\alpha = (\Pi_e^2 + \Pi_i^2)/\omega^2$$
$$\Pi_e^2 = 4\pi n_e e^2/m_e$$
$$\Pi_i^2 = 4\pi n_i Z^2 e^2/m_i$$

$\Omega_e = e\,B_0/m_e c$ = electron cyclotron frequency
$\Omega_i = Z\,e\,B_0/m_i c$ = ion cyclotron frequency
ω = angular frequency of the wave
$B_0 = |\mathbf{B}_0|$
e(or Ze) = magnitude of electron (or ion) charge in esu units
$m_{e,i}$ = electron or ion mass in grams
$n_{e,i}$ = electron or ion number density, cm^{-3}
θ = angle between the propagation direction (i.e., that of $\mathbf{k}$) and $\mathbf{B}_0$

The dispersion equation is quadratic in n^2, and hence there are in general two modes. In particular, for $\theta = 0$: $n^2 = R$ (with right-handed circular polarization), and $n^2 = L$ (with left-handed circular polarization); and for $\theta = \pi/2$: $n^2 = RL/S$ (the extraordinary mode), and $n^2 = P$ (the ordinary mode). Polarization, left- or right-handed, is defined, for positive ω, with respect to the direction of the ambient magnetic field $\mathbf{B}_0$. *Resonances* occur when $n^2 = \pm\infty$, and *cutoffs*, when $n^2 = 0$. Resonances: (1) $\theta = 0$: the *electron cyclotron resonance* at $\omega = \Omega_e$ ($R \to \pm\infty$); and the *ion cyclotron resonance* at $\omega = \Omega_i$ ($L \to \pm\infty$). (2) $\theta = \pi/2$: the *lower hybrid resonance* at ω_{LH}, where ω_{LH} approximately satisfies

$$\omega_{LH}^{-2} = (\Omega_i^2 + \Pi_i^2)^{-1} + (\Omega_i\Omega_e)^{-1}$$

and the *upper hybrid resonance* at ω_{UH}, where ω_{UH} approximately satisfies

$$\omega_{UH}^2 = \Omega_e^2 + \Pi_e^2$$

Numerous modes of plasma waves have been investigated extensively, but only those that are frequently encountered in the geophysical environment are mentioned below. All these modes are defined in a homogeneous plasma. The plasma in the magnetosphere cannot necessarily be regarded as being homogeneous, and drift waves may play an important role in inducing instabilities, but these and other instabilities are not discussed here since they are not as yet adequately understood under geophysical conditions.

Magnetohydrodynamic Waves ($\omega \ll \Omega_i$)

$$n^2 = 1 + \gamma \qquad \text{for the fast mode (compressional wave)} \qquad (5h\text{-}1)$$

$$n^2 \cos^2\theta = 1 + \gamma \qquad \text{for the slow mode (Alfvén wave)} \qquad (5h\text{-}2)$$

where

$$\gamma = 4\pi(n_i m_i + n_e m_e)\frac{c^2}{B_0^2} \approx \frac{4\pi\rho c^2}{B_0^2} \qquad \rho = \text{plasma density}$$

the characteristic velocity $c/\sqrt{1+\gamma}$ is called the Alfvén velocity. When $\gamma \gg 1$, this reduces to $B_0/\sqrt{4\pi\rho}$, which is V_A given in Sec. 5h-29. The slow mode disappears at $\omega = \Omega_i$. The fast mode exists at frequencies above Ω_i and continues on to the whistler mode. The phase velocity of the fast mode is isotropic.

Ion Cyclotron Waves ($\omega \lesssim \Omega_i$). The slow wave in Eq. (5h-2) has a characteristic dispersion relation just below the ion cyclotron frequency. In the neighborhood of $\omega = \Omega_i$, n^2 for the two modes are approximately

$$n^2 \approx \frac{\gamma}{1 + \cos^2\theta} \qquad \text{for the fast mode} \qquad (5h\text{-}3)$$

$$n^2 \cos^2\theta \approx \gamma(1 + \cos^2\theta)\frac{\Omega_i^2}{\Omega_i^2 - \omega^2} \qquad \text{for the slow mode} \qquad (5h\text{-}4)$$

The ion cyclotron resonance appears in the slow mode; for this mode the dispersion relation can be rewritten as

$$\omega^2 \approx \Omega_i^2\left(1 + \frac{\Pi_i^2}{k_\parallel^2 c^2} + \frac{\Pi_i^2}{k_\parallel^2 c^2 + k_\perp c^2}\right)^{-1}$$

where $k_\parallel$ and $k_\perp$ denote the components of $\mathbf{k}$ parallel and perpendicular to $\mathbf{B}_0$, respectively. Waves in this mode are called ion cyclotron waves.

The "Whistler" Mode ($\Omega_i < \omega < \Omega_e$). The branch that is an extension of the fast mode in Eq. (5h-1) is called the *whistler mode*. The term "whistler mode" originates from the circumstance that whistlers (Sec. 5h-33) propagate in this mode; however, the use of this term is not limited to the propagation of natural whistlers. The refractive index for this mode is approximately given by

$$n^2 = 1 - \frac{\alpha\omega}{\omega - \Omega_e \cos\theta}$$

provided that

$$\Omega_e \sin^4\theta \ll 4\omega^2(1-\alpha)^2\cos^2\theta \qquad \text{(quasi-longitudinal propagation)}$$

and that

$$\Omega_e^2 \sin^2\theta \ll |2\omega^2(1-\alpha)|$$

where $\alpha = \Pi_e^2/\omega^2$ in the present approximation. For $\theta = 0$ the wave has a right-handed, circular polarization, and exhibits a resonance at $\omega = \Omega_e$, i.e., the electron cyclotron frequency; the wave becomes evanescent above Ω_e.

Ion Acoustic and Electrostatic Ion Cyclotron Waves. In a plasma with finite electron and ion temperatures T_e and T_i, respectively, *ion acoustic waves* propagate in the direction parallel to $\mathbf{B}_0$ with a dispersion relation

$$\frac{1}{\omega^2} = \frac{1}{k^2}\frac{m_i}{Z\kappa T_e} + \frac{1}{\Pi_i^2}$$

if β_e ($\equiv 8\pi n_e \kappa T_e/B_0^2$) is small and if $T_i \ll T_e$, where κ is the Boltzmann constant. If T_i is comparable to T_e, the ion thermal velocity becomes comparable to the wave phase velocity, and the wave will be strongly Landau-damped.

For $\theta \neq 0$, and for frequencies above Ω_i but close to it, the *electrostatic ion cyclotron wave* can propagate, under certain conditions, with a dispersion relation

$$\omega^2 \approx \Omega_i^2 + k_\perp^2 \frac{Z\kappa T_e}{m_i}$$

where $k_\perp$ is the component of $\mathbf{k}$ perpendicular to $\mathbf{B}_0$.

Electrostatic Plasma Waves. In the absence of a magnetic field, a plasma resonates electrostatically with the frequency Π_e ($\approx \sqrt{4\pi n_e e^2/m_e}$, ignoring the ion motion). This frequency is called the *Langmuir* or *plasma frequency.* The reflection of radio waves from the ionosphere is due to this resonance (Sec. 5h-19).

5h-31. Geomagnetic Pulsations [100–102]. Rapid geomagnetic fluctuations with periods approximately from 0.2 sec to 10 min (or roughly 5 to 0.001 Hz in frequency) are generally referred to as *pulsations* or *micropulsations.* Fluctuations (or signals) in the frequency range 3,000 to 3 Hz are often grouped under ELF (extra low frequency) waves and those with frequencies <3 Hz under ULF (ultrahigh frequency); in this scheme of nomenclature pulsations may be regarded as being ULF phenomena. However, various names and corresponding abbreviations have been used for different groups of pulsations; these include: "transient" (*pt*), "continuous" (*pc*), "giant" (*pg*) pulsations and "pearls" (*pp*). The International Association of Geomagnetism and Aeronomy recommended in 1963 adoption of a scheme in which pulsations are divided into two groups: regular (and continuous) and irregular pulsations, denoted by *pc* and *pi*, respectively. These groups are divided further into several subgroups according to the following scheme:

Type	*Range of period, sec*
Regular (continuous) pulsations	
pc 1	0.2– 5
pc 2	5 – 10
pc 3	10 – 45
pc 4	45 –150
pc 5	150 –600
Irregular pulsations	
pi 1	1 – 40
pi 2	40 –150

However, the above classification is solely based on periods and should be considered as a tentative scheme, which is likely to be modified as the sources of different types of pulsations become identified. The morphological characteristics of pulsations are extremely complex, and only a few types of pulsations are described below.

Quasi-sinusoidal continuous oscillations with frequencies about 0.1 to 5 Hz and with "beating" characteristics have been interpreted as hydromagnetic emissions from

the magnetosphere. Because of the resemblance of the appearance of their amplitude variations to pearls on a necklace they are often called "pearls." In a frequency-time display (i.e., sonagram) these pulsations often consist of discrete repetitive emissions of rising frequency, but those of irregular structure or of other types are also observed. In the case of repetitive emissions, wave packets are observed alternatingly at magnetically conjugate points (i.e., at the northern and southern feet of a line of magnetic force), indicating that the hydromagnetic waves propagate along the lines of force back and forth between two hemispheres. These wave packets are likely to be generated by cyclotron instabilities involving protons in the magnetosphere.

There has been much discussion of the possibility of eigenoscillations of the magnetosphere, but such oscillations have not as yet been positively identified. Because of the inhomogeneities of the plasma density and of the axial asymmetry of the magnetic field, the oscillation of the magnetosphere is likely to be extremely complex. Nevertheless some types of pulsations appear to be caused by regional oscillations of the magnetosphere. In particular, large-amplitude damped oscillations observed in the auroral zones (Sec. 5h-10) appear to be due to oscillations of the magnetic field lines embedded in the auroral zones; small-amplitude ($<1\ \gamma$) regular, continuous oscillations belonging to *pc* 2, 3 may be due to oscillations of a large volume of the magnetosphere predominantly on the dayside. Transverse, regular oscillations with amplitudes of 1 to 10 γ and with periods from 1 to several minutes have been observed by a satellite at a distance of about 7 earth radii from the earth, mostly on geomagnetically quiet days and in the dayside magnetosphere.

Another group of magnetic oscillations observed in the magnetosphere has periods from a fraction of one second to several seconds and amplitudes less than 1 γ; these are probably the same oscillations as those observed at high latitudes and grouped under hydromagnetic emissions or *pc* 1. Many other groups of magnetic oscillations will probably be found in the magnetosphere, but satellite observations of pulsations have just begun, and classifications and studies of generation mechanisms are still left for the future.

At high latitudes irregular pulsations (*pi* 1 and 2) with wide ranges of periods and amplitudes are observed in association with magnetic and auroral disturbances; some of these pulsations are closely related to particle precipitations. Hence these pulsations can be regarded as part of the disturbance phenomena discussed in Secs. 5h-10 and 5h-11.

5h-32. ELF (Extra Low Frequency) Waves [100,101]. The main sources for natural electromagnetic signals or emissions observed on the earth in the ELF range, 3 to 300 Hz, are "*sferics*" (or *atmospherics*), *earth-ionosphere cavity resonances*, and *ELF emissions*.

Sferics [85]. Emissions from lightning, when VLF signals are filtered, have slow tails which contain frequencies below a few hundred hertz. These signals propagate in a "cavity" between the earth and the ionosphere, as if in a waveguide, with low attenuation and characteristic dispersion.

Cavity Resonances [103]. Wavelengths of *ELF* signals can be of the order of several thousand kilometers, and such long-wavelength signals can cause resonances in the earth-ionosphere cavity; these resonances are sometimes called the *Schumann resonances*. Typical resonance frequencies for the first five modes are near 8, 14, 20, 27, and 32 Hz. These resonance frequencies vary with conditions in the lower ionosphere (the lower D and C regions), and exhibit diurnal variations normally of the order of a fraction of one hertz. Harmonics of the resonance as high as the 11th (~70 Hz) have been observed. Appreciable shifts in the resonance frequencies are seen during severe ionospheric disturbances and at the times of high-altitude nuclear explosions.

ELF Emissions [104,105]. Electromagnetic emissions of natural origin, normally classed under VLF phenomena (Sec. 5h-33), often extend into the ELF range; thus

the division between VLF and ELF is somewhat artificial. Particularly in cases where the propagation is in the whistler mode, the designation ELF is often only a convenient way of indicating the low-frequency portion of the VLF phenomena. In the magnetosphere the most prominent emission in the total ELF-VLF range, in the sense of integrated occurrence and intensity in space and time, falls in the range 300 to 3,000 Hz and has been called *ELF hiss*. Satellite observations indicate that this signal is almost continuously present at altitudes >300 km in the late morning hours along L shells (Sec. 5h-22), corresponding to invariant latitudes of 55 to 65° [106,89]. The percentage of time of occurrence as a function of signal intensity decreases markedly for **E** between 60 and 180 μv meter^{-1} (rms) at an altitude of 700 km [89]. Similarly, for samples distributed between 240 and 2,700 km altitude, occurrences decrease markedly for **B** between 2 and 6 milligammas (rms) [106]. Although occurrence is most frequent near 60° invariant latitude in the late morning, the total region of frequent occurrence (e.g., >10 percent of the time) extends throughout the dayside hours 6h to 18h local time and invariant latitudes 50 to 70°. Although the ELF hiss signal is relatively steady in the sense that rapid changes in intensity are absent, it is frequently accompanied by a second signal, called *ELF chorus*. The chorus signals consist of a long series of wave packets, each having a duration of the order of one second, and the characteristic that the frequency rises with time within each packet. The time-space distribution of ELF hiss and chorus observed from satellites, and the fact that their occurrence at the earth's surface is less common and more erratic, suggest that these signals are repeatedly reflected from hemisphere to hemisphere from ionospheric levels. There is evidence that this reflection occurs roughly at the altitude where the signal frequency equals the proton gyrofrequency (but is presumably affected by the presence of heavier ions), and that the effective gyrofrequency also acts as a low-frequency cutoff [107]. Some signal apparently reaches the earth's surface through mode-coupling mechanisms.

ELF signals of a more transient nature than the ELF hiss, noted above, are encountered in the auroral-belt and polar-cap regions. These are frequently associated with irregularities (Sec. 5h-17) in electron density and electric fields when observed by satellites [89]. Although most ELF emissions propagating in the whistler mode are believed to be generated in the magnetosphere, it has been suggested that a strong signal near 700 Hz in the auroral zone might be caused by proton cyclotron radiation in the ionosphere [108].

Part of the energy of the ELF (and VLF) emission from a lightning impulse propagates upward into the ionosphere and sometimes triggers a *proton whistler* [109]. In a frequency-time display, such as in a sonogram, a proton whistler has a dispersion characteristic of slowly rising frequency that asymtotically approaches the proton cyclotron frequency at the point of observation by a satellite. The frequency at which this proton whistler originates in the frequency-time display is an extension of the trace that corresponds to the "electron whistler," to be discussed in Sec. 5h-33. Proton whistlers are thought to be ion cyclotron waves (Sec. 5h-30).

5h-33. Whistlers and VLF Emissions [100,104]. *Whistlers* are electromagnetic signals in audio frequencies originating from lightning strokes. They are called whistlers because of their whistling sound when converted into audio signals. Whistlers typically have a descending tone from above 10 to 1 kHz; however, the upper limit can be as high as 30 kHz or even higher, and the lowest may extend to the ELF or even ULF range. The duration of a whistler is about one second, but some whistlers last only for a fraction of a second and others for two or three seconds. Whistlers propagate in the whistler mode (Sec. 5h-30), which is roughly a guided mode along the magnetic field lines. Only a slight electron density gradient is required to make tubes of magnetic force act like ducts for whistler propagation. Ducted whistlers often propagate back and forth between the two hemispheres repeatedly. The

group velocity, with which wave energy propagates, has a maximum at a frequency of say, f_1, and decreases for frequencies above and below f_1. Therefore, in a frequency-time display (e.g., in a sonogram) a signal trace for a whistler that traveled a long distance shows the earliest arrival at f_1 and a gradual delay in arrival time as f departs from f_1 above and below. A whistler exhibiting such a dispersion characteristic is called a *nose whistler*, and the frequency f_1 of the minimum delay, the *nose frequency*. In a homogeneous medium f_1 is $\frac{1}{4}f_H$, where f_H is the electron cyclotron frequency ($= \Omega_e/2\pi$). The group delay time, say t, for a whistler that has traversed a one-hop path from one hemisphere to the other can be approximately expressed by

$$t = Df^{-\frac{1}{2}}$$

for f well below the nose frequency; the constant D, called the *dispersion constant* or simply the *dispersion*, is given approximately by

$$D = (2c)^{-1} \int_{\text{path}} (f_p/f_H^{\frac{1}{2}})\, ds \qquad \text{sec}^{\frac{1}{2}}$$

where c is the velocity of light, and f_p the electron plasma frequency ($= \Pi_e/2\pi$). Apart from a constant, the integrand reduces to $(n_e/B)^{\frac{1}{2}}$ where n_e is the electron density, and B the magnetic field intensity. Thus various models for the electron density in the magnetosphere can be tested by comparing the observed D with the calculated values. Studies of electron densities in the magnetosphere by means of whistlers have shown that there is a "knee" in the electron density profile at several earth radii and that the electron density drops substantially beyond this distance (Sec. 5h-21). Whistlers have been detected by satellites at various altitudes in the magnetosphere, and their behaviors are now being investigated in detail.

In addition to whistlers, there are other types of emissions in the VLF range; these are called *VLF emissions*. Several types of these emissions are observed in close association with whistlers, suggesting that they are triggered by the latter. VLF emissions may last steadily for minutes, or even hours, or may occur in bursts; converted to sound waves, they may produce a hissing sound or show a musical tone. (A division of hiss into ELF and VLF groups is entirely artificial.) VLF emissions are most frequently observed at middle and high latitudes, and indicate similarity in occurrence and form at magnetically conjugate areas in the northern and southern hemispheres. Such mechanisms as electron cyclotron radiation and Čerenkov radiation have been suggested for the origin of VLF emissions. The possibility of these VLF waves having significant interaction with energetic particles in the radiation belt has been extensively investigated [56,62].

References

1. Chapman, S., and J. Bartels: "Geomagnetism," Clarendon Press, Oxford, 1940, 1951, 1962 (corrected).
2. Matsushita, S., and W. H. Campbell, eds.: "Physics of Geomagnetic Phenomena," Academic Press, Inc., New York, 1967.
3. Vestine, E. H., L. LaPorte, I. Lange, and W. E. Scott: The Geomagnetic Field, Its Description and Analysis, *Carnegie Inst. Wash. Publ.* 580, 1947.
4. Adopted at the International Association of Geomagnetism and Aeronomy Symposium on Description of the Earth's Magnetic Field, Washington, D.C., Oct. 22–25, 1968.
5. Vestine, E. H.: Chap. II-2, p. 181, in ref. 2.
6. Cain, J. C.: Personal communication December, 1968.
7. Vestine, E. H., L. Laporte, C. Cooper, I. Lange, W. C. Hendrix: Description of the Earth's Main Magnetic Field and Its Secular Change, *Carnegie Inst. Wash. Publ.* 578, 1947.
8. Symposium on Magnetism of the Earth's Interior: *J. Geomag. Geoel.*, **17** (3–4) (1965).
9. Cain, J. C., and S. J. Hendricks: The Geomagnetic Secular Variation 1900–1965, *NASA Tech. Note* TN-D-4527, 1968.

10. Cain, J. C., S. J. Hendricks, R. A. Langel, and W. V. Hudson: *J. Geomag. Geoel.* **19,** 335 (1967).
11. Beloussov, V. V., P. J. Hart, B. C. Heezen, H. Kuno, V. A. Magnitsky, T. Nagata, A. R. Ritsema, and G. P. Woollard, eds.: The Earth's Crust and Upper Mantle, *Am. Geophys. Union Geophys. Monograph* 13, Washington, D.C., 1969; in particular, chap. 5.
12. Serson, P. H., and W. L. W. Hannaford: *J. Geophys. Research* **62,** 1 (1957).
13. McCormac, B. M., ed.: Aurora and Airglow, *Proc. NATO Study Inst.*, 1966, Reinhold Book Corporation, New York, 1967.
14. McCormac, B. M., ed.: Aurora and Airglow, *Proc. NATO Study Inst.*, 1968, Reinhold Book Corp., New York, 1969.
15. Harang, L.: *Terrest. Magnetism and Atmospheric Elec.*, **51,** 353 (1946).
16. Fukushima, N.: *J. Fac. Sci. Univ., Tokyo,* **8,** 293 (1953).
17. Heppner, J. P.: Ref. 13, p. 75.
18. Akasofu, S.-I.: *Space Sci. Rev.* **4,** 498 (1965).
19. McCormac, B. M., ed.: Earth's Particles and Fields, *Proc. NATA Advanced Study Inst.*, 1967, Reinhold Book Corporation, New York, 1968.
20. Frank, L. A., Ref. 19, p. 67.
21. Hoffman, R. A., and L. J. Cahill, Jr.: *J. Geophys. Research* **73,** 6711 (1968).
22. Sugiura, M.: *Ann. IGY* **35,** 9. Pergamon Press, New York, 1964.
23. Sugiura, M., and S. J. Hendricks: *NASA Tech. Note*, NASA TN D-5748, 1970.
24. Mead, G. D.: *J. Geophys. Research* **69,** 1181 (1964).
25. Sugiura, M.: *J. Geophys. Research* **70,** 4151 (1965).
26. Bartels, J.: *Ann. IGY* **4,** 227, Pergamon Press, New York, 1957.
27. Lincoln, J. V.: Chap. I-3, p. 67, in ref. 2.
28. Davis, T. N., and M. Sugiura: *J. Geophys. Research* **71,** 785 (1966).
29. Rikitake, T.: "Electromagnetism and the Earth's Interior," Elsevier Publishing Company, Amsterdam, 1966.
30. Price, A. T.: Chap. II 3, p. 235, in ref. 2.
31. Madden, T. R., and C. M. Swift, Jr.: In ref. 11.
32. Ratcliffe, J. A., ed.: "Physics of the Upper Atmosphere," Academic Press, Inc., New York, 1960.
33. Rishbeth, H.: *Rev. Geophys.* **6,** 33 (1968).
34. Donahue, T. M.: *Science,* **159,** 489 (1968).
35. Cohen, R.: Chap. III-4, p. 561, in ref. 2.
36. Herman, J. R.: *Rev. Geophys.* **4,** 255 (1966).
37. Symposium on Upper Atmospheric Winds, Waves, and Ionospheric Drifts, IAGA Assembly, 1967; *J. Atmospheric and Terrest. Phys.* **30**(5), (1968).
38. Smith, E. K., and S. Matsushita, eds.: "Ionospheric Sporadic E," Pergamon Press, Oxford, 1962.
39. Smith, E. K., Jr.: Chap. III-5, p. 615, in ref. 2.
40. Baker, W. G., and D. F. Martyn: *Phil. Trans. Roy. Soc. London,* Ser. A, **246,** 281 (1953).
41. Chapman, S.: *Nuovo Cimento* **4** (suppl.), 1385 (1956).
42. Ratcliffe, J. A.: "The Magneto-ionic Theory and its Applications to the Ionosphere," Cambridge University Press, London, 1959.
43. Hess, W. N., and G. D. Mead, eds.: "Introduction to Space Science," 2d ed., Gordon and Breach, Science Publishers, Inc., New York, 1968.
44. King, J. W., and W. S. Newman, eds.: "Solar-Terrestrial Physics," Academic Press, Inc., New York, 1967.
45. Heppner, J. P., M. Sugiura, T. L. Skillman, B. G. Ledley, and M. Campbell: *J. Geophys. Research* **72,** 5417 (1967).
46. Ness, N. F.: Ref. 44, p. 57.
47. Heppner, J. P.: In ref. 14.
48. Ness, N. F., K. W. Behannon, S. C. Cantarano, and C. S. Scearce: *J. Geophys. Research* **72,** 927 (1967).
49. Ness, N. F., C. S. Scearce, and S. C. Cantarano: *J. Geophys. Research* **72,** 3769 (1967).
50. Wolfe, J. H., R. W. Silva, D. D. McKibbin, and R. H. Mason: *J. Geophys. Research* **72,** 4577 (1967).
51. Sugiura, M., T. L. Skillman, B. G. Ledley, and J. P. Heppner: Presented at International Symposium on the Physics of the Magnetosphere, Washington, D.C., September, 1968. Sugiura, M.: In "The World Magnetic Survey 1957–1969," IAGA Bulletin No. 28.
52. Bame, S. J.: Ref. 19, p. 373.
53. Vasyliunas, V. M.: *J. Geophys. Research* **73,** 2839 (1968).
54. Carpenter, D. L.: *J. Geophys. Research* **71,** 693 (1966).

55. McCormac, B. M., ed.: Radiation Trapped in the Earth's Magnetic Field, *Proc. Advanced Study Inst.*, Bergen, 1965, D. Reidel Publishing Co., Dordrecht, Holland, 1966.
56. Hess, W. N.: "The Radiation Belt and Magnetosphere," Blaisdell Publishing Company, a division of Ginn and Company, Waltham, Mass., 1968.
57. Van Allen, J. A., and L. A. Frank: *Nature* **183,** 430 (1959).
58. Brown, W. L., L. J. Cahill, L. R. Davis, C. E. McIlwain, and C. S. Roberts: *J. Geophys. Research* **73,** 153 (1968).
59. Williams, D. J., J. F. Arens, and L. J. Lanzerotti: *J. Geophys. Research* **73,** 5673 (1968).
60. Symposium on Scientific Effects of Artificially Introduced Radiations at High Altitudes, *J. Geophys. Research* **64**(8), 865 (1959).
61. Collected Papers on the Artificial Radiation Belt from the July 9, 1962, Nuclear Detonation. W. N. Hess, ed., *J. Geophys Research* **68**(3), 605 (1963).
62. Kennel, C. F., and H. E. Petschek: *J. Geophys. Research* **71,** 1 (1966).
63. Anderson, K. A.: *J. Geophys. Research* **70,** 4741 (1965); P. Serlemitsos: *ibid.* **71,** 61 (1966); A. Konradi: *ibid.* 2317; E. W. Hones, Jr., S. Singer, and C. S. R. Rao: *ibid.* **73,** 7339 (1968).
64. McDiarmid, I. B., and J. R. Burrows: *J. Geophys. Research* **70,** 3031 (1965).
65. Northrop, T. G.: "The Adiabatic Motion of Charged Particles," Interscience Publishers, a division of John Wiley & Sons, Inc., New York, 1963.
66. Alfvén, H., and C.-G. Fälthammar: "Cosmical Electrodynamics," Clarendon Press, Oxford, 1963.
67. McIlwain, C. E.: Ref. 55, p. 45.
68. Hines, C. O.: *Space Sci. Rev.* **3,** 342 (1964).
69. Cowling, T. G.: "Magnetohydrodynamics," Interscience Publishers, Inc., New York, 1957.
70. Dungey, J. W.: "Cosmic Electrodynamics," Cambridge University Press, London, 1958.
71. Gold, T.: *J. Geophys. Research* **64,** 1219 (1959).
72. Axford, W. I., and C. O. Hines: *Can. J. Phys.* **39,** 1433 (1961).
73. Taylor, H. E., and E. H. Hones: *J. Geophys. Research* **70,** 3605 (1965).
74. Obayshi, T., and A. Nishida: *Space Sci. Rev.* **8,** 3 (1968).
75. Parker, E. N.: "Interplanetary Dynamical Processes," Interscience Publishers, a division of John Wiley & Sons, Inc., New York, 1963.
76. Axford, W. I.: *Space Sci. Rev.*, **8,** 331 (1968).
77. Snyder, C. W., M. Neugebauer, and U. R. Rao: *J. Geophys. Research* **68,** 6361 (1963).
78. Hundhausen, A. J., J. R. Asbridge, S. J. Bame, H. E. Gilbert, and I. B. Strong: *J. Geophys. Research* **72,** 87 (1967).
79. Frank, L. A.: (abstract) *Trans. Am. Geophys. Union* **49,** 262 (1968).
80. Wilcox, J. M.: *Space Sci. Rev.* **8,** 258 (1968).
81. Ness, N. F., C. S. Scearce, J. B. Seek, and J. M. Wilcox: "Space Research," vol. VI, p. 581, R. L. Smith-Rose, ed., Spartan Books, Washington, D.C., 1966.
82. McCracken, K. G., and N. F. Ness: *J. Geophys. Research* **71,** 3315 (1966).
83. Colburn, D. S., and C. P. Sonett: *Space Sci. Rev.* **5,** 439 (1966).
84. Spreiter, J. R., A. L. Summers, and A. Y. Alksne: *Planet. Space Sci.* **14,** 223 (1966).
85. Coroniti, S. C., ed.: Problems of Atmospheric and Space Electricity, *Proc. 3d Intern. Conf. Atmospheric and Space Elec.*, 1963, Elsevier Publishing Company, Amsterdam, 1965.
86. Smith, L. G., ed.: Recent Advances in Atmospheric Electricity, *Proc. 2d Conf. Atmospheric Elec.*, Pergamon Press, New York, 1958.
87. Fahleson, U.: *Space Sci. Rev.* **7,** 238 (1967).
88. Haerendel, G., R. Liist, and E. Rieger: *Planet. Space Sci.* **15,** 1 (1967).
89. Aggson, T. L., J. P. Heppner, N. C. Maynard, and D. S. Evans: Personal Communications; presentations at International Symposium on the Physics of the Magnetosphere, September, 1968.
90. Wescott, E. M., J. Stolarik, and J. P. Heppner: *Trans. Am. Geophys. Union* **49,** 155 (1968).
91. Davis, T. N.: In ref. 14.
92. Wescott, E. M., and K. B. Mather: *J. Geophys. Research* **70,** 29 (1965).
93. Maeda, H.: *J. Geomag. Geoelec.* **7,** 121 (1955).
94. Kern, J. W.: In ref. 2.
95. Chamberlain, J. W.: "Physics of the Aurora and Airglow," Academic Press, Inc., New York, 1961.
96. Tidman, D. A.: *J. Geophys. Research* **72,** 1799 (1967).
97. Ferraro, V. C. A., and C. Plumpton: "An Introduction to Magneto-fluid Mechanics," Oxford University Press, London, 1961.

98. Stix, T. H.: "The Theory of Plasma Waves," McGraw-Hill Book Company, New York, 1962.
99. Akhiezer, A. I., I. A. Akhiezer, R. V. Polovin, A. G. Sitenko, and K. N. Stepanov: "Collective Oscillations in a Plasma," tr. H. S. H. Massey, tr. ed. R. J. Tayler, The MIT Press, Cambridge, Mass., 1967.
100. Bleil, D. F., ed.: "Natural Electromagnetic Phenomena below 30 kc/s," Plenum Press, Plenum Publishing Corporation, New York, 1964.
101. Campbell, W. H.: Ref. 2, p. 822.
102. Troitskaya, V. A.: Ref. 44, p. 213.
103. Madden, T., and W. Thompson: *Rev. Geophys.* **3**, 211 (1965).
104. Helliwell, R. A.: "Whistlers and Related Ionospheric Phenomena," Stanford University Press, Stanford, Calif., 1965.
105. Gurnett, D. A.: Ref. 19, p. 349.
106. Taylor, W. W. L., and D. A. Gurnett: *J. Geophys. Research* **73**, 5615 (1968).
107. Gurnett, D. A., and T. B. Burns: *Univ. Iowa Preprint* 68-28, Department of Physics and Astronomy, 1968.
108. Egeland, A., G. Gustafsson, S. Olsen, J. Aarons, and W. Barron: *J. Geophys. Research* **70**, 1070 (1065).
109. Gurnett, D. A., S. D. Shawhan, N. M. Brice, and R. L. Smith: *J. Geophys. Research* **70**, 1665 (1965).